Journal of Biotechnology 147 (2010) 17–30

Contents lists available at ScienceDirect

Journal of Biotechnology

journal homepage: www.elsevier.com/locate/jbiotec

Dynamic modeling of *Escherichia coli* metabolic and regulatory systems for amino-acid production

Yoshihiro Usuda[a,*], Yosuke Nishio[a], Shintaro Iwatani[a], Stephen J. Van Dien[b,1], Akira Imaizumi[b], Kazutaka Shimbo[b], Naoko Kageyama[b], Daigo Iwahata[b], Hiroshi Miyano[b], Kazuhiko Matsui[a]

[a] *Fermentation and Biotechnology Laboratories, Ajinomoto Co., Inc., 1-1 Suzuki-cho, Kawasaki-ku, Kawasaki 210-8681, Japan*
[b] *Life Science Institute, Ajinomoto Co., Inc., Kawasaki, Japan*

ARTICLE INFO

Article history:
Received 3 September 2009
Received in revised form 14 January 2010
Accepted 18 February 2010

Keywords:
Amino-acid production
Dynamic modeling
Escherichia coli
Metabolic network
Regulatory network

ABSTRACT

Our aim is to construct a practical dynamic-simulation system that can model the metabolic and regulatory processes involved in the production of primary metabolites, such as amino acids. We have simulated the production of glutamate by transient batch-cultivation using a model of *Escherichia coli* central metabolism. Kinetic data were used to produce both the metabolic parts of the model, including the phosphotransferase system, glycolysis, the pentose-phosphate pathway, the tricarboxylic acid cycle, the glyoxylate shunt, and the anaplerotic pathways, and the regulatory parts of the model, including regulation by transcription factors, cyclic AMP receptor protein (CRP), making large colonies protein (Mlc), catabolite repressor/activator (Cra), pyruvate dehydrogenase complex repressor (PdhR), and acetate operon repressor (IclR). RNA polymerase and ribosome concentrations were expressed as a function of the specific growth rate, μ, corresponding to the changes in the growth rate during batch cultivation. Parameter fitting was performed using both extracellular concentration measurements and *in vivo* enzyme activities determined by ^{13}C flux analysis. By manual adjustment of the parameters, we simulated the batch fermentation of glucose or fructose by a wild-type strain (MG1655) and a glutamate-producing strain (MG1655 Δ*sucA*). The differences caused by the carbon source, and by wild-type and glutamate-producing strains, were clearly shown by the simulation. A sensitivity analysis revealed the factors that could be altered to improve the production process. Furthermore, an *in silico* deletion experiments could suggested the existence of uncharacterized regulation. We concluded that our simulation model could function as a new tool for the rational improvement and design of metabolic and regulatory networks.

1. Introduction

Primary metabolites are important industrial products, which can generally be produced by fermentation processes. Amino acids, which are used as seasonings, food additives, and fine chemicals, are important primary metabolites. Among the amino acids, glutamate (GLU) is used as a flavor enhancer, and is produced throughout the world in quantities of over 1,500,000 metric tonnes per year. Improvements of the fermentation processes for primary metabolites are thus of great importance to industry, and they are promising targets for metabolic engineering (Bongaerts et al., 2001; de Graaf et al., 2001; Kimura, 2003). Amino acids are mainly produced by bacterial strains such as *Corynebacterium glutamicum* and *Escherichia coli* (Leuchtenberger et al., 2005; Wendisch et al., 2006). *E. coli* is a well-known model organism that is used to produce several industrial primary metabolites. The use of this bacterium has economic advantages due to its fast growth and substrate consumption rates. Furthermore, compared with most organisms *E. coli* has more abundant biochemical, molecular biological, and post-genomic information.

The goals of systems biology are to understand complex biological systems, and to modify and redirect metabolic and regulatory systems based on quantitative predictions with the aid of mathematical models (Goryanin et al., 2006; Ishii et al., 2004; Stelling, 2004). Metabolic flux analysis (MFA) using ^{13}C-labeling has become a powerful method for quantifying intracellular reaction rates within a metabolic network, and for elucidating the *in vivo* metabolic state of cells during the fermentation process (Iwatani et al., 2008; Sauer, 2006; Wittmann, 2002). By contrast, dynamic simulation of cell metabolism is expected to become a useful method for analyzing and elucidating not just metabolic state but all of the transient *in vivo* cellular bioprocesses. However, these types of simulation are challenging, largely because the kinetic parameters that describe the enzymatic reactions and the regulatory events are difficult to determine, and can sometimes differ from the physiological

* Corresponding author. Tel.: +81 44 244 7119; fax: +81 44 210 5727.
E-mail address: yoshihiro_usuda@ajinomoto.com (Y. Usuda).
[1] Present address: Genomatica Inc., San Diego, USA.

0168-1656/$ – see front matter © 2010 Elsevier B.V. All rights reserved.
doi:10.1016/j.jbiotec.2010.02.018

Table 1
Kinetic-rate equations.

PTS

$$\text{PTS1}: v = \frac{k_f[\text{EI}][\text{PEP}]}{K_{m\text{PEP}}+[\text{PEP}]} - \frac{k_r[\text{EI-P}][\text{Pyr}]}{K_{m\text{Pyr}}+[\text{Pyr}]}$$

$$\text{PTS2}: v = k_f[\text{EI-P}][\text{HPr}] - k_r[\text{EI}][\text{HPr-P}]$$

$$\text{PTS3}: v = k_f[\text{HPr-P}][\text{IIA}^{\text{Glc}}] - k_r[\text{HPr}][\text{IIA}^{\text{Glc}}\text{-P}]$$

$$\text{PTS4}: v = k_f[\text{IIA}^{\text{Glc}}\text{-P}][\text{IICB}^{\text{Glc}}] - k_r[\text{IIA}^{\text{Glc}}][\text{IICB}^{\text{Glc}}\text{-P}]$$

$$\text{PTS5}: v = \frac{k_f[\text{IICB}^{\text{Glc}}\text{-P}][\text{Glc}_{\text{xt}}]}{K_{m\text{Glc}}+[\text{Glc}_{\text{xt}}]}$$

PGI

$$v = \frac{[\text{PGI}](k_f[\text{G6P}]/K_{m\text{G6P}} - k_r[\text{F6P}]/K_{m\text{F6P}})}{1+[\text{G6P}]/K_{m\text{G6P}}+[\text{F6P}]/K_{m\text{F6P}}}$$

PFK

$$v = \frac{k[\text{PFK}]([\text{F6P}]/K_{m\text{F6P}})^n[\text{ATP}]/K_{m\text{ATP}}}{(1+([\text{F6P}]/K_{m\text{F6P}})^n)(1+[\text{ATP}]/K_{m\text{ATP}})}$$

FBA

$$v = \frac{k_f k_r[\text{FBA}]([\text{FDP}]-[\text{GA3P}][\text{DHAP}]/K_{eq})}{k_r K_{m\text{FDP}}+k_r[\text{FDP}]+k_f K_{m\text{DHAP}}[\text{GA3P}]/K_{eq}+k_f K_{m\text{GA3P}}[\text{DHAP}]/K_{eq}+k_r[\text{FDP}][\text{GA3P}]/K_{i\text{GA3P}}+k_f[\text{GA3P}][\text{DHAP}]/K_{eq}}$$

TPI

$$v = \frac{[\text{TPI}](k_f[\text{GA3P}]/K_{m\text{GA3P}} - k_r[\text{DHAP}]/K_{m\text{DHAP}})}{1+[\text{GA3P}]/K_{m\text{GA3P}}+[\text{DHAP}]/K_{m\text{DHAP}}}$$

GAP

$$v = \frac{[GAP](k_f[\text{GA3P}][\text{NAD}^+][\text{Pi}]/K_{m\text{GA3P}}K_{m\text{NAD}^+}K_{m\text{Pi}} - k_r[13\text{DPG}][\text{NADH}]/K_{m13\text{DPG}}K_{m\text{NADH}})}{(1+[\text{GA3P}]/K_{m\text{GA3P}})(1+[Pi]/K_{m\text{Pi}})+[13\text{DPG}]/K_{m13\text{DPG}}(1+[\text{NAD}^+]/K_{m\text{NAD}^+}+[\text{NADH}]/K_{m\text{NADH}})}$$

PGK

$$v = \frac{[\text{PGK}](k_f[13\text{DPG}][\text{ADP}]/K_{m13\text{DPG}}K_{m\text{ADP}} - k_r[3\text{PG}][\text{ATP}]/K_{m3\text{PG}}K_{m\text{ATP}})}{(1+[13\text{DPG}]/K_{m13\text{DPG}}+[3\text{PG}]/K_{m3\text{PG}})(1+[\text{ADP}]/K_{m\text{ADP}}+[\text{ATP}]/K_{m\text{ATP}})}$$

PGM

$$v = \frac{[\text{PGM}](k_f[3\text{PG}]/K_{m3\text{PG}} - k_r[2\text{PG}]/K_{m2\text{PG}})}{1+[3\text{PG}]/K_{m3\text{PG}}+[2\text{PG}]/K_{m2\text{PG}}}$$

ENO

$$v = \frac{[\text{ENO}](k_f[2\text{PG}]/K_{m2\text{PG}} - k_r[\text{PEP}]/K_{m\text{PEP}})}{1+[2\text{PG}]/K_{m2\text{PG}}+[\text{PEP}]/K_{m\text{PEP}}}$$

PK

$$v = \frac{k[\text{PK}]([\text{PEP}]/K_{m\text{PEP}})^n([\text{ADP}]/K_{m\text{ADP}})}{(1+([\text{PEP}]/K_{m\text{PEP}})^n)(1+[\text{Pyr}]/K_{m\text{Pyr}})}$$

G6PD

$$v = \frac{k[\text{G6PD}][\text{G6P}][\text{NADP}^+]}{([\text{G6P}]+K_{m\text{G6P}})([\text{NADP}^+]+K_{m\text{NADP}^+})}$$

6PGD

$$v = \frac{k[\text{6PGD}][\text{6PGC}][\text{NADP}^+]}{([\text{6PGC}]+K_{m\text{6PGC}})([\text{NADP}^+]+K_{m\text{NADP}^+})}$$

RPI

$$v = \frac{[\text{RPI}](k_f[\text{R5P}]/K_{m\text{R5P}} - k_r[\text{RL5P}]/K_{m\text{RL5P}})}{1+[\text{R5P}]/K_{m\text{R5P}}+[\text{RL5P}]/K_{m\text{RL5P}}}$$

RPE

$$v = \frac{[\text{RPE}](k_f[\text{RL5P}]/K_{m\text{RL5P}} - k_r[\text{X5P}]/K_{m\text{X5P}})}{1+[\text{RL5P}]/K_{m\text{RL5P}}+[\text{X5P}]/K_{m\text{X5P}}}$$

TAL

$$v = \frac{[\text{TAL}](k_f[\text{E4P}][\text{F6P}]/K_{m\text{E4P}}K_{m\text{F6P}} - k_r[\text{S7P}][\text{GA3P}]/K_{m\text{S7P}}K_{m\text{GA3P}})}{(1+[\text{E4P}]/K_{m\text{E4P}}+[\text{S7P}]/K_{m\text{S7P}})(1+[\text{F6P}]/K_{m\text{F6P}}+[\text{GA3P}]/K_{m\text{GA3P}})}$$

TKT

$$\text{TKTI}: v = \frac{[\text{TKT}](k_f[\text{R5P}][\text{X5P}]/K_{m\text{R5P}}K_{m\text{X5P}} - k_r[\text{GA3P}][\text{S7P}]/K_{m\text{GA3P}}K_{m\text{S7P}})}{(1+[\text{R5P}]/K_{m\text{R5P}}+[\text{GA3P}]/K_{m\text{GA3P}})(1+[\text{X5P}]/K_{m\text{X5P}}+[\text{S7P}]/K_{m\text{S7P}})}$$

$$\text{TKTII}: v = \frac{[\text{TKT}](k_f[\text{X5P}][\text{E4P}]/K_{m\text{X5P}}K_{m\text{E4P}} - k_r[\text{F6P}][\text{GA3P}]/K_{m\text{F6P}}K_{m\text{GA3P}})}{(1+[\text{X5P}]/K_{m\text{X5P}}+[\text{F6P}]/K_{m\text{F6P}})(1+[\text{E4P}]/K_{m\text{E4P}}+[\text{GA3P}]/K_{m\text{GA3P}})}$$

PDH

$$v = \frac{k[\text{PDH}]([\text{Pyr}]/K_{m\text{Pyr}})^n([\text{NAD}^+]/K_{m\text{NAD}^+})}{(1+([\text{ACCoA}]/K_{m\text{ACCoA}})^n)(1+[\text{NAD}^+]/K_{m\text{NAD}^+})}$$

CS

$$v = \frac{k[\text{CS}][\text{ACCoA}][\text{OAA}]}{K_{i\text{ACCoA}}K_{m\text{OAA}}+K_{m\text{OAA}}[\text{ACCoA}]+K_{m\text{ACCoA}}[\text{OAA}]+[\text{ACCoA}][\text{OAA}]}$$

ACN

$$v = \frac{[\text{ACN}](k_f[\text{CIT}]/K_{m\text{CIT}} - k_r[\text{ICIT}]/K_{m\text{ICIT}})}{1+[\text{CIT}]/K_{m\text{CIT}}+[\text{ICIT}]/K_{m\text{ICIT}}}$$

ICDH

$$v_f = \frac{k[\text{ICDH}][\text{ICIT}][\text{NADP}^+]}{K_{i\text{ICIT}}K_{m\text{NADP}^+}+K_{m\text{NADP}^+}[\text{ICIT}]+K_{m\text{ICIT}}[\text{NADP}^+]+[\text{ICIT}][\text{NADP}^+]}$$

$$v_r = \frac{k[\text{ICDH}][\text{AKG}][\text{NADPH}][\text{CO}_2]}{C+\text{CP}_1[\text{AKG}]+\text{CP}_2[\text{NADPH}]+\text{CP}_3[\text{CO}_2]+K_{m\text{AKG}}[\text{NADPH}][\text{CO}_2]+K_{m\text{NADPH}}[\text{AKG}][\text{CO}_2]+K_{m\text{CO}_2}[\text{AKG}][\text{NADPH}]+[\text{AKG}][\text{NADPH}][\text{CO}_2]}$$

$$v = v_f - v_r$$

KGDH

$$v = \frac{k[\text{KGDH}]([\text{AKG}]+\alpha[\text{AKG}]^2/K_2)}{K_{mS1}+[\text{AKG}]+[\text{AKG}]^2/K_2}$$

SCS

$$v = \frac{[\text{SCS}]\left(k_f[\text{SUCCoA}][\text{ADP}][\text{Pi}]/K_{m\text{SUCCoA}}K_{m\text{ADP}}K_{m\text{Pi}} - k_r[\text{SUCC}][\text{ATP}][\text{CoA}]/K_{m\text{SUCC}}K_{m\text{SDP}}K_{m\text{CoA}}\right)}{(1+[\text{SUCCoA}]/K_{m\text{SUCCoA}})(1+[\text{Pi}]/K_{m\text{Pi}})+[\text{SUCC}]/K_{m\text{SUCC}}[(1+[\text{ATP}]/K_{m\text{ATP}})(1+[\text{CoA}]/K_{m\text{CoA}})+[\text{ADP}]/K_{m\text{ADP}}]}$$

SDH/FRD

Table 1 (*Continued*).

$$v = \frac{[\mathrm{SDH/FRD}](k_f[\mathrm{SUCC}]/K_{m\mathrm{SUCC}} - k_r[\mathrm{FUM}]/K_{m\mathrm{FUM}})}{1+[\mathrm{SUCC}]/K_{m\mathrm{SUCC}}+[\mathrm{FUM}]/K_{m\mathrm{FUM}}}$$

FUMA

$$v = \frac{[\mathrm{FUMA}](k_f[\mathrm{FUM}]/K_{m\mathrm{FUM}} - k_r[\mathrm{MAL}]/K_{m\mathrm{MAL}})}{1+[\mathrm{FUM}]/K_{m\mathrm{FUM}}+[\mathrm{MAL}]/K_{m\mathrm{MAL}}}$$

MDH

$$v = \frac{[\mathrm{MDH}](k_f[\mathrm{MAL}][\mathrm{NAD}^-]/K_{m\mathrm{MDH}}K_{m\mathrm{NAD}^+} - k_r[\mathrm{OAA}][\mathrm{NADH}]/K_{m\mathrm{OAA}}K_{m\mathrm{NADH}})}{(1+[\mathrm{MAL}]/K_{m\mathrm{MAL}}+[\mathrm{OAA}]/K_{m\mathrm{OAA}})(1+[\mathrm{NAD}^+]/K_{m\mathrm{NAD}^+}+[\mathrm{NADH}]/K_{m\mathrm{NADH}})}$$

FBP

$$v = \frac{k[\mathrm{FBP}]([\mathrm{FDP}]/K_{m\mathrm{FDP}})}{(1+[\mathrm{FDP}]/K_{m\mathrm{FDP}})(1+[\mathrm{AMP}]/K_{i\mathrm{AMP}})}$$

PPS

$$v = \frac{[\mathrm{PPS}](k_f[\mathrm{PYR}][\mathrm{ATP}]/K_{m\mathrm{PYR}}K_{m\mathrm{ATP}} - k_r[\mathrm{PEP}][\mathrm{AMP}][\mathrm{Pi}]/K_{m\mathrm{PEP}}K_{m\mathrm{AMP}}K_{m\mathrm{Pi}})}{[(1+[\mathrm{PEP}]/K_{m\mathrm{PEP}})(1+[\mathrm{Pi}]/K_{m\mathrm{Pi}})+[\mathrm{PYR}]/K_{m\mathrm{PYR}}][(1+[\mathrm{AMP}]/K_{m\mathrm{AMP}})+[\mathrm{ATP}]/K_{m\mathrm{ATP}}]}$$

PEPC

$$v = \frac{k[\mathrm{PEPC}][\mathrm{PEP}][\mathrm{CO_2}]/K_{m\mathrm{PEP}}K_{m\mathrm{CO_2}}}{(1+[\mathrm{PEP}]/K_{m\mathrm{PEP}})(1+[\mathrm{CO_2}]/K_{m\mathrm{CO_2}})(1+[\mathrm{ASP}]/K_{i\mathrm{ASP}})(1+[\mathrm{MAL}]/K_{i\mathrm{MAL}})}$$

ME

$$v = \frac{k[\mathrm{ME}]([\mathrm{MAL}]/K_{m\mathrm{MAL}})^n([\mathrm{NAD}^+]/K_{m\mathrm{NAD}^+})}{(1+([\mathrm{MAL}]/K_{m\mathrm{MAL}})^n)(1+[\mathrm{NAD}^+]/K_{m\mathrm{NAD}^+})}$$

PCK

$$v = \frac{[\mathrm{PCK}](k_f[\mathrm{OAA}][\mathrm{ATP}]/K_{m\mathrm{OAA}}K_{m\mathrm{ATP}} - k_r[\mathrm{PEP}][\mathrm{ADP}][\mathrm{CO_2}]/K_{m\mathrm{PEP}}K_{m\mathrm{ADP}}K_{m\mathrm{CO_2}})}{[(1+[\mathrm{PEP}]/K_{m\mathrm{PEP}})(1+[\mathrm{CO_2}]/K_{m\mathrm{CO_2}})+[\mathrm{OAA}]/K_{m\mathrm{OAA}}][(1+[\mathrm{ADP}]/K_{m\mathrm{ADP}})+[\mathrm{ATP}]/K_{m\mathrm{ATP}}]}$$

ICL

$$v = \frac{k[\mathrm{ICL}][\mathrm{ICIT}]}{K_{m\mathrm{ICIT}}(1+[\mathrm{3PG}]/K_{i3\mathrm{PG}})+[\mathrm{ICIT}]}$$

MS

$$v = \frac{k[\mathrm{MS}]([\mathrm{ACCoA}]/K_{m\mathrm{ACCoA}})^n([\mathrm{GLX}]/K_{m\mathrm{GLX}})}{(1+([\mathrm{ACCoA}]/K_{m\mathrm{ACCoA}})^n)(1+[\mathrm{GLX}]/K_{m\mathrm{GLX}})}$$

ICDP/ICDK

$$\mathrm{ICDP}: v = \frac{k[\mathrm{ICDP/ICDK}][\mathrm{ICDH}](K_{\mathrm{A3PG}}+\beta[\mathrm{3PG}])/(K_{a3\mathrm{PG}}+\beta[\mathrm{3PG}])}{K_{m\mathrm{ICDH}}+[\mathrm{ICDH}]}$$

$$\mathrm{ICDK}: v = \frac{k[\mathrm{ICDP/ICDK}]([\mathrm{ICDH}]/K_{m\mathrm{ICDH}})}{(1+[\mathrm{ICDH}]/K_{m\mathrm{ICDH}})(1+[\mathrm{3PG}]/K_{i3\mathrm{PG}})}$$

CYA

$$v = \frac{k[\mathrm{CYA}]([\mathrm{ATP}]/K_{m\mathrm{ATP}})}{(1+[\mathrm{ATP}]/K_{m\mathrm{ATP}})(1+[\mathrm{ATP}]/K_{i\mathrm{ATP}})}$$

CYA activation

$$[\mathrm{activated\ CYA}] = \frac{([\mathrm{CYA}]^{tot}+[\mathrm{IIA^{Glc}\text{-}P}]^{tot}+K_d^{\mathrm{CYAA}} - \sqrt{([\mathrm{CYA}]^{tot}+[\mathrm{IIA^{Glc}\text{-}P}]^{tot}+K_d^{\mathrm{CYAA}})^2 - 4[\mathrm{CYA}]^{tot}+[\mathrm{IIA^{Glc}\text{-}P}]^{tot}+K_d^{\mathrm{CYAA}}]^{tot}[\mathrm{IIA^{Glc}\text{-}P}]^{tot}})}{2}$$

$$[\mathrm{CYA}] = [\mathrm{CYA}]^{tot} - [\mathrm{activated\ CYA}]$$

CDP

$$v = \frac{k_f[\mathrm{CDP}][\mathrm{cAMP}]}{K_{mc\mathrm{AMP}}+[\mathrm{cAMP}]}$$

CEX

$$v = k[\mathrm{cAMP}]$$

FRUK

$$v = \frac{[\mathrm{FruK}](k_f[\mathrm{F1P}][\mathrm{ATP}]/K_{m\mathrm{F1P}}K_{m\mathrm{ATP}} - k_r[\mathrm{FDP}][\mathrm{ADP}]/K_{m\mathrm{FDP}}K_{m\mathrm{ADP}})}{(1+[\mathrm{F1P}]/K_{m\mathrm{F1P}}+[\mathrm{FDP}]/K_{m\mathrm{FDP}})(1+[\mathrm{ATP}]/K_{m\mathrm{ATP}}+[\mathrm{ADP}]/K_{m\mathrm{ADP}})}$$

GDH

$$v = \frac{[\mathrm{GDH}](k_f[\mathrm{AKG}][\mathrm{NADPH}]/K_{m\mathrm{AKG}}K_{m\mathrm{NADPH}} - k_r[\mathrm{GLU}][\mathrm{NADP}^+]/K_{m\mathrm{GLU}}K_{m\mathrm{NADP}^+})}{(1+[\mathrm{AKG}]/K_{m\mathrm{AKG}}+[\mathrm{GLU}]/K_{m\mathrm{GLU}})(1+[\mathrm{NADPH}]/K_{m\mathrm{NADPH}}+[\mathrm{NADP}^+]/K_{m\mathrm{NADP}^+})}$$

ASPAT

$$v = \frac{[\mathrm{ASPAT}](k_f[\mathrm{ASP}][\mathrm{AKG}]/K_{m\mathrm{ASP}}K_{m\mathrm{AKG}} - k_r[\mathrm{OAA}][\mathrm{GLU}]/K_{m\mathrm{ASP}}K_{m\mathrm{AKG}})}{(1+[\mathrm{ASP}]/K_{m\mathrm{ASP}}+[\mathrm{OAA}]/K_{m\mathrm{OAA}})(1+[\mathrm{AKG}]/K_{m\mathrm{AKG}}+[\mathrm{GLU}]/K_{m\mathrm{GLU}})}$$

Excretion of AcOH, FORM, and GLU

$$\mathrm{AcOH}: v = k[\mathrm{AcOH}]$$

$$\mathrm{FORM}: v = k[\mathrm{FORM}]$$

$$\mathrm{GLU}: v = k[\mathrm{GLU}]$$

states inside cells (Ovádi and Srere, 1996). There have been many attempts to overcome these major obstacles (Goryanin et al., 2006; Ishii et al., 2004). So far, examples of the large-scale kinetic modeling of *E. coli* central metabolism include studies by Chassagnole et al. (2002), who reported a dynamic simulation including the phosphotransferase system (PTS), glycolysis, and pentose-phosphate pathway but excluding the regulatory network, and by Wang et al. (2001), who described the kinetics of *E. coli* glycolysis in combination with sucrose PTS expression modeling.

We previously reported on an *E. coli* stoichiometric model and a method of theoretical MFA, which predicted the target metabolic flux based on multivarient analysis (Van Dien et al., 2006). We have also developed practical analytical methods for determining metabolic fluxes using a ^{13}C-substrate, in which metabolites inside the cell that are derived from the labeled substrate can be analyzed during the industrial fermentation process (Iwatani et al., 2007). Additionally, we constructed a dynamic model of the kinetics of the sugar-uptake system (PTS) and its regulatory pathways in *E. coli*, which we used to predict the sugar-uptake rate together with experimental validations (Nishio et al., 2008).

In the current study we expanded our previous model, and constructed a large-scale metabolic and regulatory model of *E. coli* central metabolism, which included the metabolic enzymes of the PTS, glycolysis, the pentose-phosphate pathway, the tricarboxylic acid (TCA) cycle, anaplerotic enzymes, and the glyoxylate shunt, as well as transcriptional regulation due to cyclic AMP receptor protein (CRP), making large colonies protein (Mlc), catabolite repressor/activator (Cra), pyruvate dehydrogenase complex repressor (PdhR), and acetate operon repressor (IclR). In total, 45 enzymatic reactions were modeled based on Michaelis–Menten kinetics using data mainly from experiments reported in the literature. The transcription and translation of 46 genes were modeled

Table 2
Model of gene expression.

Transcription factor

Crp

$$[\text{CRP}-\text{cAMP}]^{tot} = \frac{([\text{CRP}]^{tot}+[\text{cAMP}]^{tot}+K^{CRP}_{\text{dcAMP}}-\sqrt{([\text{CRP}]^{tot}+[\text{cAMP}]^{tot}+K^{\text{CRP}}_{\text{dcAMP}})^2-4[\text{CRP}]^{tot}[\text{cAMP}]^{tot}})}{2}$$

$$[\text{P-CRP-cAMP}] = \frac{([\text{CRP-cAMP}]^{tot}+[P^{\text{CRP}}]^{tot}+K^{\text{CRP}}_{d}-\sqrt{([\text{CRP-cAMP}]^{tot}+[P^{\text{CRP}}]^{tot}+K^{\text{CRP}}_{d})^2-4[\text{CRP-cAMP}]^{tot}[P^{\text{CRP}}]^{tot}})}{2}$$

$$[\text{CRP-cAMP}] = [\text{CRP-cAMP}]^{tot} - [\text{P-CRP-cAMP}]$$

Mlc

$$[\text{Mlc-IICB}^{\text{Glc}}] = \frac{([\text{Mlc}]^{tot}+[\text{IICB}^{\text{Glc}}]^{tot}+K^{\text{Mlc}}_{\text{dIICB}}-\sqrt{([\text{Mlc}]^{tot}+[\text{IICB}^{\text{Glc}}]^{tot}+K^{\text{Mlc}}_{\text{dIICB}})^2-4[\text{Mlc}]^{tot}[\text{IICB}^{\text{Glc}}]^{tot}})}{2}$$

$$[\text{Mlc}] = [\text{Mlc}]^{tot} - [\text{Mlc}-\text{IICB}^{\text{Glc}}]$$

Cra

$$[\text{Cra-F1P}] = \frac{([\text{Cra}]^{tot}+[\text{F1P}]^{tot}+K^{\text{Cra}}_{\text{dF1P}}-\sqrt{([\text{Cra}]^{tot}+[\text{F1P}]^{tot}+K^{\text{Cra}}_{\text{dF1P}})^2-4[\text{Cra}]^{tot}[\text{F1P}]^{tot}})}{2}$$

$$[\text{Cra}] = [\text{Cra}]^{tot} - [\text{Cra}-\text{F1P}]$$

PdhR

$$[\text{PdhR-PEP}] = \frac{([\text{PdhR}]^{tot}+[\text{PYR}]^{tot}+K^{\text{PdhR}}_{\text{dPYR}}-\sqrt{([\text{PdhR}]^{tot}+[\text{PYR}]^{tot}+K^{\text{PdhR}}_{\text{dPYR}})^2-4[\text{PdhR}]^{tot}[\text{PYR}]^{tot}})}{2}$$

$$[\text{PdhR}] = [\text{PdhR}]^{tot} - [\text{PdhR}-\text{PYR}]$$

IclR

$$[\text{IclR-PEP}] = \frac{([\text{IclR}]^{tot}+[\text{PEP}]^{tot}+K^{\text{IclR}}_{\text{dPEP}}-\sqrt{([\text{IclR}]^{tot}+[\text{PEP}]^{tot}+K^{\text{IclR}}_{\text{dPEP}})^2-4[\text{IclR}]^{tot}[\text{PEP}]^{tot}})}{2}$$

$$[\text{IclR}] = [\text{IclR}]^{tot} - [\text{IclR}-\text{PEP}]$$

Transcription without regulation (NoTF)

$$\frac{d[\text{mRNA}_{\text{gene}}]}{dt} = k^{\text{base}}_{\text{gene}}[\text{RNAP}\sigma^{\text{D}}][P_{\text{gene}}]^{tot} - (k^{d\text{RNA}}_{\text{gene}}+\mu)[\text{mRNA}_{\text{gene}}]$$

Transcription with one transcription factor (TF1)

$$\frac{d[\text{mRNA}_{\text{gene}}]}{dt} = \frac{k^{\text{base}}_{\text{gene}}+k^{\text{Rep}}_{\text{gene}}[\text{TF}]/K^{\text{TFR}}_{\text{dgene}}}{1+[\text{TF}]/K^{\text{TFR}}_{\text{dgene}}}[\text{RNAP}\sigma^{D}][P_{\text{gene}}]^{tot} - (k^{\text{dRNA}}_{\text{pgene}}+\mu)[\text{mRNA}_{\text{gene}}]$$

Transcription with two transcription factors

crp

$$\frac{d[\text{mRNA}_{\text{crp}}]}{dt} = \frac{k^{\text{base}}_{\text{crp}}+k^{\text{CRPCRP}}_{\text{crp}}([\text{CRP}-\text{cAMP}]/K^{\text{CRP}}_{dcrp2}+[\text{CRP}-\text{cAMP}]^2/K^{\text{CRP}}_{\text{dcrp1}}K^{\text{CRP}}_{\text{dcrp2}})}{1+[\text{CRP}-\text{cAMP}]/K^{\text{CRP}}_{\text{dcrp1}}+[\text{CRP}-\text{cAMP}]/K^{\text{CRP}}_{\text{dcrp2}}+[\text{CRP}-\text{cAMP}]^2/K^{\text{CRP}}_{\text{dcrp1}}K^{\text{CRP}}_{\text{dcrp2}}}[\text{RNAP}\sigma^{\text{D}}][P_{\text{crp}}]^{tot} - (k^{\text{dRNA}}_{\text{crp}}+\mu)[\text{mRNA}_{\text{crp}}]$$

mlc

$$\frac{d[\text{mRNA}_{\text{mlc}}]}{dt} = \frac{k^{\text{base}}_{\text{mlc}}+k^{\text{CRP}}_{\text{mlc}}[\text{CRP}-\text{cAMP}]/K^{\text{CRP}}_{\text{dmlc}}/+k^{\text{Mlc}}_{\text{mlc}}([\text{Mlc}]/K^{\text{Mlc}}_{\text{dmlc}}+[\text{CRP}-\text{cAMP}][\text{Mlc}]/K^{\text{CRP}}_{\text{dmlc}}K^{\text{Mlc}}_{\text{dmlc}})}{1+[\text{CRP}-\text{cAMP}]/K^{\text{CRP}}_{\text{dmlc}}+[\text{Mlc}]/K^{\text{Mlc}}_{\text{dmlc}}+[\text{CRP}-\text{cAMP}][\text{Mlc}]/K^{\text{CRP}}_{\text{dmlc}}K^{\text{Mlc}}_{\text{dmlc}}}[\text{RNAP}\sigma^{\text{D}}][P_{\text{crp}}]^{tot} - (k^{\text{dRNA}}_{\text{mlc}}+\mu)[\text{mRNA}_{\text{mlc}}]$$

ptsHI-crr

$$\frac{d[\text{mRNA}_{\text{ptsHI}}]}{dt} = \frac{k^{\text{base}}_{\text{ptsHIP1}}(1+[\text{Mlc}]/K^{\text{mlc}}_{\text{dptsHI}})+k^{\text{CRP}}_{\text{ptsHIP0}}[\text{CRP}-\text{cAMP}]/K^{\text{CRP}}_{\text{dptsHI}}+k^{\text{CRP}}_{\text{ptsHIP1}}([\text{CRP}-\text{cAMP}]/K^{\text{CRP}}_{\text{dptsHI}}+[\text{CRP}-\text{cAMP}][\text{Mlc}]/K^{\text{CRP}}_{\text{dptsHI}}K^{\text{mlc}}_{\text{dptsHI}})}{1+[\text{CRP}-\text{cAMP}]/K^{\text{CRP}}_{\text{dptsHI}}+[\text{Mlc}]/K^{\text{Mlc}}_{\text{dptsHI}}+[\text{CRP}-\text{cAMP}][\text{Mlc}]/K^{\text{CRP}}_{\text{dptsHI}}K^{\text{Mlc}}_{\text{dptsHI}}}[\text{RNAP}\sigma^{\text{D}}][P_{\text{ptsHI}}]^{tot} - (k^{d\text{RNA}}_{\text{ptsHI}}+\mu)[\text{mRNA}_{\text{ptsHI}}]$$

ptsG

$$\frac{d[\text{mRNA}_{\text{ptsG}}]}{dt} = \frac{k^{\text{CRP}}_{\text{ptsG}}[\text{CRP}-\text{cAMP}]/K^{\text{CRP}}_{\text{dptsG}}+k^{\text{CRPMlc}}_{\text{ptsG}}[\text{CRP}-\text{cAMP}][\text{Mlc}]/K^{\text{CRP}}_{\text{dptsG}}K^{\text{Mlc}}_{\text{dptsG}}}{1+[\text{CRP}-\text{cAMP}]/K^{\text{CRP}}_{\text{dptsG}}+[\text{Mlc}]/K^{\text{Mlc}}_{\text{dptsG}}+[\text{CRP}-\text{cAMP}][\text{Mlc}]/K^{\text{CRP}}_{\text{dptsG}}K^{\text{Mlc}}_{\text{dptsG}}}[P_{\text{ptsG}}]^{tot}[\text{RNAP}\sigma^{\text{D}}] - (k^{d\text{RNA}}_{\text{ptsG}}+\mu)[\text{mRNA}_{\text{ptsG}}]$$

aceBAK

$$\frac{d[\text{mRNA}_{\text{aceBAK}}]}{dt} = \frac{k^{\text{base}}_{\text{aceBAK}}+k^{\text{Cra}}_{\text{aceBAK}}[\text{Cra}]/K^{\text{Cra}}_{\text{daceBAK}}}{1+[\text{Cra}]/K^{\text{Cra}}_{\text{daceBAK}}+[\textit{IclR}]/K^{\text{IclR}}_{\text{daceBAK}}+[\text{Cra}][\text{IclR}]/K^{\text{Cra}}_{\text{daceBAK}}K^{\text{IclR}}_{\text{daceBAK}}}[\text{RNAP}\sigma^{\text{D}}][P_{\text{gene}}]^{tot} - (k^{\text{dRNA}}_{\text{gene}}+\mu)[\text{mRNA}_{\text{gene}}]$$

Translation

$$\frac{d[\text{Protein}]}{dt} = k^{\text{trans}}[\text{Ribosome}][\text{mRNA}_{\text{gene}}] - (k^{\text{deg}}+\mu)[\text{Protein}]$$

Translation with transcriptional attenuation

$$\frac{d[\text{Protein}]}{dt} = k^{\text{trans}}[\text{Ribosome}][\text{mRNA}_{\text{gene}}]T_{\text{Protein}} - (k^{\text{deg}}+\mu)[\text{Protein}]$$

IIA^{Glc}

$$\frac{d[\text{IIA}^{\text{Glc}}]}{dt} = k^{\text{trans}}[\text{Ribosome}]([\text{mRNA}_{\text{crr}}]+[\text{mRNA}_{\text{ptsHI}}]T_{\text{EI}}) - (k^{\text{deg}}+\mu)[\text{EI}]$$

KGDH

$$\frac{d[\text{KGDH}]}{dt} = k^{\text{trans}}[\text{Ribosome}]([\text{mRNA}_{\text{sucABCD}}]+[\text{mRNA}_{\text{sdhCDAB}}])T_{\text{KGDH}} - (k^{\text{deg}}+\mu)[\text{KGDH}]$$

SCS

$$\frac{d[\text{SCS}]}{dt} = k^{\text{trans}}[\text{Ribosome}]([\text{mRNA}_{\text{sucABCD}}]+[\text{mRNA}_{\text{sdhCDAB}}])T_{\text{SCS}} - (k^{\text{deg}}+\mu)[\text{SCS}]$$

based on known regulatory information. We investigated both GLU production and the growth of the wild-type strain using our model. GLU is produced via a simple biosynthetic pathway from α-ketoglutarate (AKG), which is part of the TCA cycle, and GLU producers can easily be obtained from the wild-type strain. The batch fermentation process involves successive transient phases, in which the cultivation is started at an initial sugar substrate concentration and is continued until the substrate becomes exhausted. During batch cultivation, the specific growth rate, μ, varies; the RNA polymerase (RNAP) and ribosome concentrations are therefore expressed as a function of μ. The metabolic fluxes determined experimentally using ^{13}C-labeled substrates were used to adjust the kinetic parameters that we judged to provide the most reliable data on the *in vivo* enzyme activities. Although the dynamic model that we have constructed inevitably includes quantitative errors, we have shown that it can accurately describe the transient fermentation processes. We have also shown that the application of sensitivity analyses and *in silico* deletion experiment using this

model are valuable for improving the productivity by means of gene amplification, deletion, and deregulation.

2. Materials and methods

2.1. Modeling

The enzymatic reactions and transport processes were modeled based largely on reversible or irreversible Michaelis–Menten-type velocity equations based on rapid equilibrium assumption and velocity equations derived from steady-state assumptions (Segel, 1975). Detailed biochemical information about each reaction that was to be modeled was collected from the literature. The kinetic-rate equations used are shown in Table 1. The binding between transcription factors and their effectors was described by algebraic equations based on the assumption of an equilibrium reaction. Gene expression was described by transcription and translation rate equations. The transcription equations for *crp*, *mlc*, *ptsHI-crr*, *ptsG*, and *aceBAK*, were defined to include regulation by two transcription factors. The Cra concentration was treated as a constant due to a lack of regulatory information. The equations used for gene expression are shown in Table 2. Details of the model are described in Supplementary Information.

2.2. Parameters and initial values

The systems parameters and metabolite concentrations used as constants in the simulation are shown in Suppl. Table 1. The dry cell weight (DCW) per optical density (OD) was obtained from measurements of the DCWs of 300 mL cultures of an *E. coli* wild-type strain MG1655, as described below, at three different time points. The cell density per OD (celldens) was set as the average of five independent experiments involving five measurements of two dilutions of the MG1655 culture broth. The cell volume (cellvol) and the cell weight (cellweight) were calculated based on the assumption that the cellvol per g DCW was 0.0025 L/g (Rohwer et al., 2000). The rate constant for translation was estimated based on the reported value of 11.03 at $\mu = 0.01\,(\mathrm{min})^{-1}$ (Lee and Bailey, 1984) and the ribosome concentration.

The initial metabolite concentrations shown in Suppl. Table 2 were taken from the literature, such as Chassagnole et al. (2002), with the exception of some estimated values. The initial values for messenger RNA (mRNA) and protein are shown in Suppl. Table 3. All of the initial values for mRNAs were set at 0. The values for initial protein concentrations were estimated from the values reported in the literature for specific activities in crude extracts and purified proteins. The total concentrations of the PTS components have been described previously (Rohwer et al., 2000), and the initial concentrations of the phosphorylated species were assumed to be 5% of the total concentrations. Membrane proteins, such as $\mathrm{IICB^{Glc}}$, which is a glucose-specific IIBC component of the PTS, were assumed to react in the cytoplasm. The modified initial values and parameters are shown in each simulation.

Suppl. Table 4 shows the parameters used for the enzymatic reactions. The parameters for phosphoglucose isomerase (PGI), triosephosphate isomerase (TPI), phosphoglycerate kinase (PGK), and enolase (ENO) were acquired from experiments (Matsui H, Nakazawa Y, and Shimazaki D, Unpublished data), except for those for the reverse reaction of ribulose phosphate 3-epimerase (RPE). The parameters used for gene expression and proteins are shown in Suppl. Table 5.

Promoter concentrations were described as the copy numbers of genes generated by μ-dependent equations, based on the formulae given by Bremer and Dennis (1996). In the current report, we have used a constant promoter concentration at $\mu = 0.01\,(\mathrm{min})^{-1}$. The number of CRP binding sites in the genome were estimated based on the assumption that approximately 200 binding sites in EcoCyc (Karp et al., 2007) are equally distributed on the genome at $\mu = 0.01\,(\mathrm{min})^{-1}$. The equations are described in the Supplementary Information. The rate constants of transcription were calculated using protein concentrations or specific enzyme activities as stationary values. In regulated genes, the rate constants of the regulated and unregulated states were estimated from the data on transcriptional activities or their protein concentrations, such as those from mutant forms of transcription factors. The mRNA degradation rates were taken from the literature if they were available, or otherwise determined based on data from microarray experiments (Selinger et al., 2003).

2.3. Simulation

MATLAB (MathWorks) for Windows was used for the simulations. Each enzymatic reaction was described as a module. Differential equations were used for the concentrations of metabolites, gene transcripts, enzymes, and transcription factors. The ode15 s of MATLAB was adopted as an ordinary differential equation (ODE) solver.

Cell growth was described as total cell volume (cellvoltot). The cellvoltot was calculated as follows from the experimental OD values:

$$\mathrm{cellvoltot} = \mathrm{cellvol} \times \mathrm{celldens} \times \mathrm{reacvol} \times \mathrm{OD}.$$

In each batch-cultivation experiment, μ was calculated from an approximation of the growth curve given by the ODs (Suppl. Table 4) at each time point. The μ value was used for calculation of the μ-dependent constants and then the ODE sets were solved. The curve fitting program, TableCurve 2D (Systat Software) was used for the approximation formulae for μ from the OD profiles, and for the specific sugar-consumption rates from the residual sugar-concentration measurements.

Rates of transcription and translation were expressed as functions of the RNAP and ribosome concentrations, respectively. RNAP functions as the holoenzyme bound by sigma factors. The rate of transcription was assumed to be dependent on the RNAP concentration bound by the growth-phase sigma factor σ^{D} [RNAP – σ^{D}]. As the value of σ^{D} has been reported to be sufficient for RNAP, and dissociation of σ^{D} from the RNAP core enzyme is relatively slow ($K^{\sigma^{\mathrm{D}}}_{\mathrm{dRNAP}} = 2.6 \times 10^{-10}$ (M)) (Jishage et al., 1996), most of the RNAP was assumed to be bound by σ^{D}. Thus, the free [RNAP – σ^{D}] that was not bound to promoters was estimated to be roughly one-third of the total RNAP concentration. The numbers of intracellular RNAP and ribosome molecules are known to be dependent on μ (Bremer and Dennis, 1996). The number of intracellular RNAP molecules was fitted by TableCurve 2D and the [RNAP – σ^{D}] was expressed as a function of μ by the following formula:

$$[\mathrm{RNAP} - \sigma^{\mathrm{D}}] = 2.64 \times 10^{-2}\mu^2 + 3 \times 10^{-4}\mu + 6.67 \times 10^{-7}.$$

The [ribosome] was expressed by the following formula as a function of μ:

$$[\mathrm{Ribosome}] = 1.90138 \times 10^{-5} + 1.37691253\ 8\mu^2 - 10.2421446\ \mu^{2.5} + 36.6287614\ 6\mu^3.$$

Biomass formation was taken into account based on the cell growth and stoichiometric matrix (Iwatani et al., 2007; Van Dien et al., 2006) by subtracting the required amount of biomass formation from the intermediate metabolite, as shown in Fig. 1. The amount required to form 1 g of dry cell was estimated from macromolecule biosynthesis (Stephanopoulos et al., 1998) and cell composition (Neidhardt and Umbarger, 1996; Pramanik and Keasling, 1997).

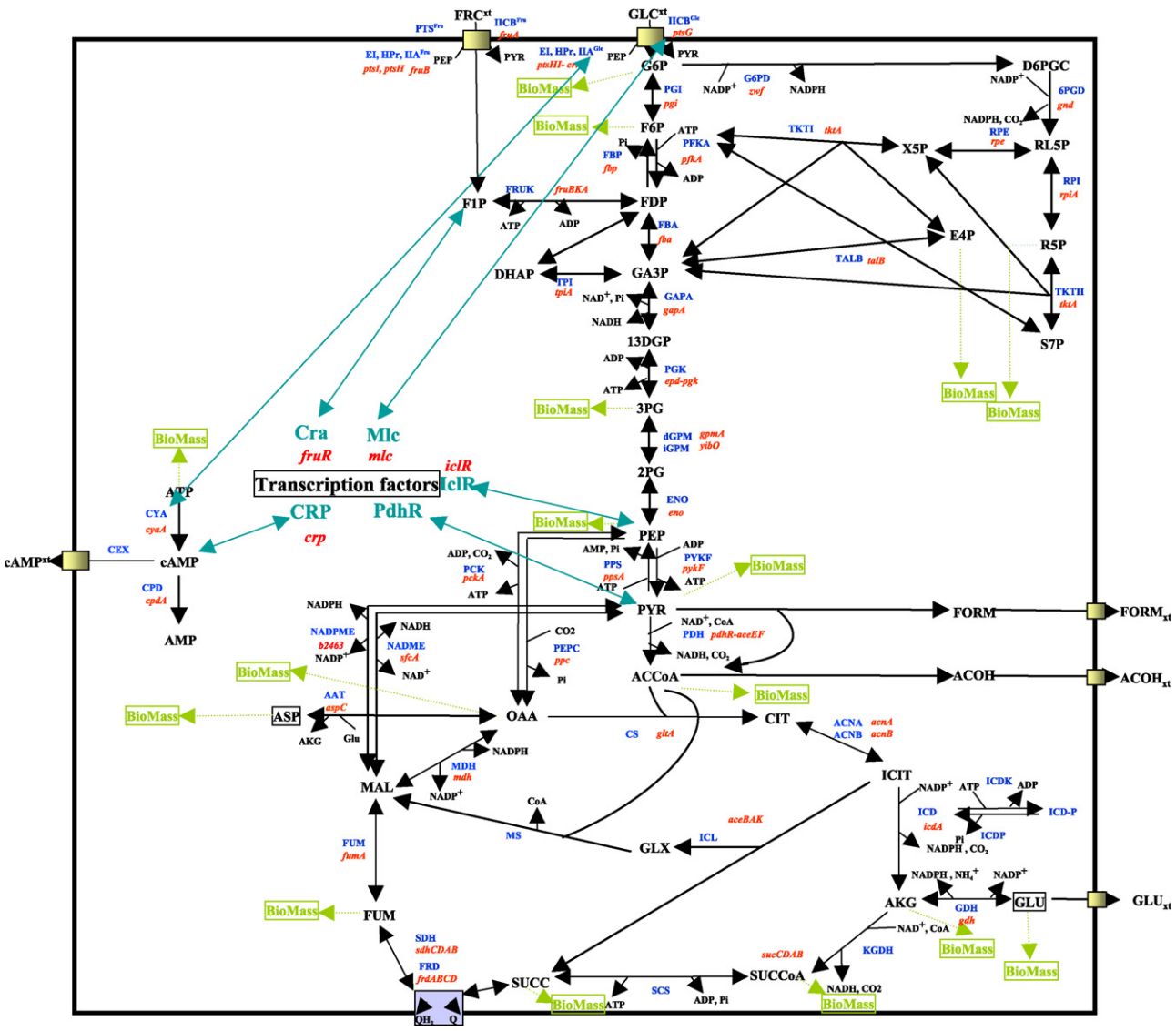

Fig. 1. Enzyme reactions, genes, and regulators modeled in this study. The metabolites shown in black and the enzymes shown in blue are represented using abbreviated names. The enzymes encoded by the genes shown in red letters were modeled in this study. Several isozymes encoded by the genes shown in black have not yet been incorporated into the model. External glucose (Glc_{xt}) is imported and metabolized. The box shows the cell membrane.

Sugar-consumption rates from approximation formulae were used to convert metabolic fluxes into *in vivo* enzyme activities (Suppl. Table 4). The cumulative generation of carbon dioxide (CO_2) was calculated from enzymatic reactions and biomass formation.

2.4. Cultivation and analysis

An *E. coli* wild-type strain (MG1655) was cultivated in L broth (Sambrook and Russell, 2001) at 37 °C until the OD reached 6. The cells were washed with saline and inoculated into 300 mL of main medium, which comprised 40 g/L (222 mM) glucose or fructose as a carbon source, 1 g/L $MgSO_4{\cdot}7H_2O$, 16 g/L $(NH_4)_2SO_4$, 1 g/L KH_2PO_4, 0.01 g/L $FeSO_4{\cdot}7H_2O$, 0.01 g/L $MnSO_4{\cdot}7H_2O$, and 2 g/L yeast extract. Cultivation was performed using a 1-L scale jar-fermentor in batch-cultivation mode with agitation control of the dissolved oxygen activity (PL) above 5% at pH 6.8 maintained by ammonium gas at 37 °C. Sampling was conducted at the following time points: 270, 420, and 540 min in the glucose culture; and 300, 510, and 600 min in the fructose culture. A GLU producer (MG1655 Δ*sucA*) derived from a wild-type strain was cultivated in main medium with 40 g/L glucose as a carbon source supplemented with 0.25 g/L Ile, Val, Leu, and DL-Met, and 0.5 g/L Lys-HCl (Imaizumi et al., 2006). Sampling was conducted at 320, 480, and 660 min. MFA was performed according to Iwatani et al. (2007) with mixed labeled compounds (1-^{13}C-glucose:U-^{13}C-glucose = 1:1 for glucose culture) as initial substrates. Samples for determining intracellular metabolites were extracted by phenol/methanol and analyzed by liquid chromatography (LC)–tandem mass spectrometry (MS/MS) with a derivatizing reagent for amino acids and organic acids. Metabolic fluxes were normalized to glucose uptake rate, which was given the value 10. The errors and confidential intervals of determined metabolic fluxes were equivalent to the results in previous report (Iwatani et al., 2007). The cumulative CO_2 generation was calculated from the CO_2 concentration that was experimentally measured by infrared gas sensor at the gas exhaust.

2.5. Sensitivity analysis

Sensitivity analysis against the concentration of excreted GLU was performed for each parameter by doubling or by reducing to one-half.

Table 3
Changes of initial values and parameters.

Variable	Name	Value	Wild-type (glucose) fold change	Wild-type (fructose) fold change	Glutamate producer fold change
CYA	Adenylate cyclase		0.7	0.7	0.5
CPD	cAMP phosphodiesterase	8.08E−06	0.3	0.3	0.4
EItot	Enzyme I	1.12E−05	0.5	0.5	0.1
EI-P	Phosphorylated EI	1.06E−05	0.5	0.5	0.1
IIAGlctot	Enzyme IIAGlc	7.69E−05	0.2	0.2	0.15
IIAGlc-P	Phosphorylated IIAGlc	7.31E−05	0.2	0.2	0.15
IICBGlctot	Enzyme IICBGlc	7.21E−06	3	2	
IICBGlcP	Phosphorylated IICBGlcP	6.85E−06	3	2	
PFKA	Phosphofructokinase I	1.42E−06	8	0.5	3.5
FBA	Fructose-16-bisphosphatate aldolase II	3.09E−05	2		0.25
PYKF	Pyruvate kinase I	2.75E−06	4	1.5	3
TKTA	Transketolase A	3.46E−06	0.25	0.25	0.25
PDH	Pyruvate dehydrogenase	3.32E−07			
CS	Citrate synthase	3.68E−06			
ACNA	Aconitase A	4.19E−06			
ACNB	Aconitase B	1.13E−05			
ICD	Isocitrate dehydrogenase	1.19E−04	0.1	0.1	0.1
ICDP	Phosphorylated isocitrate dehydrogenase	1.19E−04	0.1	0.1	0.1
KGDH	α-Ketoglutarate dehydrogenase	7.04E−06	0.5	0.5	*0*
SCS	Succinyl-CoA synthetase	3.03E−05			*0*
FBP	Fructose-16-bisphosphatase	2.55E−07		200	
PPS	Phsophoenolpyruvate synthase	3.86E−06	0.01	0.01	
PEPC	PEP carboxylase	1.89E−06	10	10	10
NADME	NAD-dependent malic enzyme	2.75E−07	0.05	0.05	
NADPME	NADP-dependent malic enzyme	1.87E−07	0.05	0.05	
ICL	Isocitrate lyase	1.20E−05			0.1
MS	Malate synthase	3.61E−06			0.1
ICDKP	Isocitrate dehydrogenase kinase/phosphatase	3.61E−08			0.1
FPrtot	Enzyme FPr	4.50E−05		1.2	
FPr-P	Phosphorylated FPr	4.28E−05		1.2	
IIAFrctot	Enzyme IIAFrc	4.50E−05		1.2	
IIAFrc-P	Phosphorylated IIAFrc	4.28E−05		1.2	
IICBFrctot	Enzyme IICBFrc	4.50E−05		1.2	
IICBFrc-P	Phosphorylated IICBFrc	4.28E−05		1.2	
GDH	NADP-specific glutamate dehydrogenase	9.95E−07	20	20	20
AAT	Aspartate aminotransferase	3.13E−06	10	10	10

Enzyme	Parameter	Value	Fold change	Fold change	Fold change
FBA	k_f	1.82E+03	10	10	10
	K_{eq}	1.00E−04	10	10	10
TPIA	k_f	3.86E+03	25	7.5	7.5
GAPA	k_f	6.34E+04	2	2	2
RPIA	k_r	4.89E+02	20	20	20
RPE	k_r	2.10E+03	5	5	5
TALB	k_f	2.10E+02	100	100	100
TKTI	k_f	8.67E+02	100	100	100
TKTII	k_r	8.95E+03	5	5	5
MDH	k_f	1.26E+03	100	100	100
FBP	K_{iAMP}	2.70E−06		100	
PCK	k_f	2.53E+02	20	20	20
MSA	k_f	3.00E+03	5	5	5
ICDP	k_f	1.90E+01	5	5	10
FRUK	k_r	5.00E+03	2.5	2.5	2.5
	K_{mFDP}	5.00E−03	0.2	0.2	0.2
GDH	k_f	2.81E+04	5	5	5
Form efflux	k_f	1.00E+00	2	2	

Gene	Parameter	Value	Fold change	Fold change	Fold change
cyaA	k^{base}_{cyaA}	2.23E+02	0.7	0.7	
	k^{CRP}_{cyaA}	9.13E+01	0.7	0.7	
cpdA	k^{base}_{cpdA}	1.28E+04	0.5	0.5	0.6
ptsG	k^{CRP}_{ptsG}	2.84E+05	0.8	1.5	1.5
	k^{CRPMIc}_{ptsG}	1.72E+03	0.8	1.5	1.5
ptsHI	T_{EI}	9.10E−02	0.025	0.05	0.015
crr	k_{crrP2}	7.57E+04	0.5	0.5	0.5
pfkA	k^{base}_{pfkA}	3.68E+03	5	0.5	1.5
	k^{Cra}_{pfkA}	1.37E+03	5	0.5	1.5
fba	k^{base}_{fba}	2.50E+04	10	4	2

Table 3 (*Continued*).

Gene	Parameter	Value	Fold change	Fold change	Fold change
gapA	k^{base}_{gapA}	6.09E+04	2	2	
pykF	k^{base}_{pykF}	8.14E+03	1.5	1.5	3
	k^{Cra}_{pykF}	2.01E+03	1.5	1.5	3
zwf	k^{base}_{zwf}	3.37E+04	2	2	2
gnd	k^{base}_{gnd}	4.40E+04	2	2	2
pdhR-aceEF	k^{base}_{pdhR}	1.28E+03	0.5	0.5	0.25
	k^{PdhR}_{pdhR}	1.95E+02	0.5	0.5	0.25
gltA	k^{base}_{gltA}	2.27E+04	4	4	1.5
acnA	k^{base}_{acnA}	1.44E+03	5	5	4
	k^{CRP}_{acnA}	5.30E+03	5	5	4
acnB	k^{base}_{acnB}	4.73E+03	5	5	4
	k^{CRP}_{acnB}	1.33E+04	5	5	4
icdA	k^{base}_{icdA}	9.70E+03	0.5	0.2	0.2
	k^{Cra}_{icdA}	3.80E+04	0.5	0.2	0.2
sucABCD	$k^{base}_{sucABCD}$	1.23E+04	8		0.8
	T_{KGDH}	4.02E−02	2	2	*0*
	T_{SCS}	6.92E−01			*0*
fbp	K^{Cra}_{dfbp}	5.00E−07		400	
	k^{base}_{fbp}	2.58E+02		400	
ppsA	k^{base}_{ppsA}	2.06E+03	0.1	0.1	
	k^{Cra}_{ppsA}	9.45E+04	0.1	0.1	
ppc	k^{base}_{ppc}	2.30E+03	10	10	10
sfcA	k^{base}_{sfcA}	4.51E+02			0.1
b2463	k^{base}_{b2463}	2.30E+02			0.1
fruBKA	k^{base}_{fruBKA}	4.09E+05		0.9	
	k^{Cra}_{fruBKA}	1.51E+04		0.9	
gdhA	k^{base}_{dghA}	1.19E+03	20	20	20
aspC	k^{base}_{aspC}	3.47E+03	10	10	10

The default changes for the GLU producer are shown in italics.

3. Results

3.1. Wild-type model and experimental validation

We constructed an *E. coli* wild-type model, the default parameters of which are shown in Suppl. Tables 2-5. To validate our model, we cultivated the *E. coli* wild-type MG1655 strain using glucose as a carbon source, according to our standard batch-cultivation mode for amino-acid production. The cultivation results are shown in Suppl. Fig. 1. The calculated metabolic fluxes are shown in Suppl. Figs. 2–4. The initial glucose (222 mM) was exhausted at approximately 10 h. The major products of cultivation were acetate and formate. Thus, both of the excretion rates of acetate and formate were used to calculate overall flux distributions. The metabolic fluxes at three phases (4.5, 7, and 9 h) were calculated and normalized (Suppl. Figs. 2–4). To make metabolic fluxes comparable to enzyme activities in simulation, the metabolic flux values were converted to enzymatic activity unit based on the experimental sugar-consumption rate. The parameters were fitted manually to adjust the enzyme activities to the metabolic fluxes, mainly due to alterations of the amounts of enzymes (initial enzyme concentrations and transcription rate constants). The enzyme kinetic parameters were altered only when acceptable results could not be obtained with these other adjustments. The altered parameters are shown in Table 3. Among the enzyme kinetic parameters, the catalytic constants of TALB, TKTI, and malate dehydrogenase (MDH) were subject to the most critical changes (100-fold change in the forward rate constant; Table 3).

The simulation results for representative metabolites and genes in a glucose culture of the wild-type strain are shown in Fig. 2 (see Suppl. Figs. 5–8 for the results for all variables). The total cell volume increased based on the experimentally measured μ (Fig. 1(A)). The external glucose and CO_2 concentrations showed good agreement with the experimental results as shown in Fig. 2(B) and (C), respectively. However, the external acetate and formate concentrations did not agree as closely with the experimental results (Fig. 2(D) and (E), respectively). The reason for the former discrepancy was that our model could not take up acetate, although the concentration decreased at later time of culture. In order to keep other intracellular metabolites in the appropriate range, the rate constants of mass action reactions for acetate and formate excretion needed to be lowered. Thus the model underpredicted both acetate and formate production. However, we succeeded in simulating all of the gene expression and enzyme reaction rates within the allowable range of metabolite concentrations, by simple manual adjustment of the parameters of the *E. coli* wild-type model.

3.2. Wild-type model with fructose as carbon source

To examine the application to other sugars, we set up a fructose culture of the wild-type strain. In the model, the PTS for fructose was added and was utilized via fructose 1-phosphate (F1P). The cultivation results and metabolic fluxes are shown in Suppl. Fig. 9 and Suppl. Figs. 10–12, respectively. The culture time was slightly extended, and the initial fructose was exhausted in 11 h. The simulation results of the fructose culture of the wild-type strain are shown in Fig. 3 (the complete results are shown in Suppl. Figs 13–16). Fructose consumption and CO_2 excretion showed good agreement with the experimental results, as shown in Fig. 3(B) and (C), respectively. However, the external acetate and formate concentrations did not agree as closely with the experimental results (Fig. 3(D) and (E), respectively).

In the glucose culture, F1P was defined by the equilibrium between F1P and fructose 1,6-diphosphate (FDP) catalyzed by fructose-1-phosphate kinase (FRUK); however, in the fructose culture, the F1P was supplied by the fructose and was simulated at a higher concentration than glucose (Fig. 2(N) and Fig. 3(N)). Expression of the *fruBAK* operon encoding PTS^{Frc} and FRUK was elevated due to deregulation of Cra. However, the catalytic constant for the forward reaction of fructose-1,6-bisphosphatase (FBP), which catalyzes gluconeogenesis from FDP to fructose 6-phosphate (F6P), needed to be increased more than 400-fold and its expression

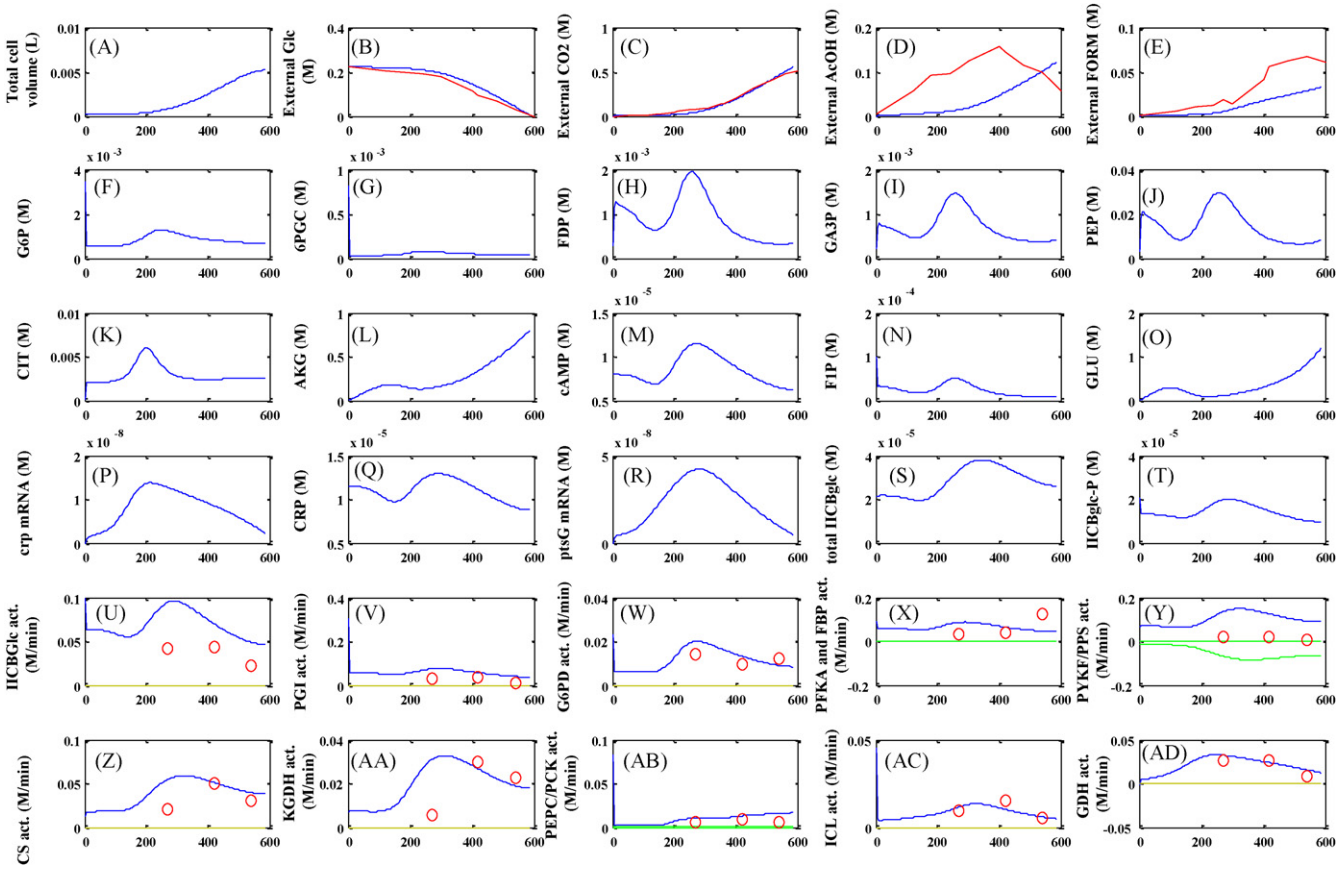

Fig. 2. Simulation of glucose culture of *E. coli* wild-type strain MG1655. (A) Total cell volume, (B) external GLC, (C) external CO_2, (D) external AcOH, (E) external FORM, (F) G6P, (G) 6PGC, (H) FDP, (I) GA3P, (J) PEP (K) CIT, (L) AKG, (M) cAMP, (N) F1P, (O) GLU, (P) *crp* mRNA, (Q) CRP, (R) *ptsG* mRNA, (S) $IICB^{Glc}$ (T) $IICB^{Glc}$-P, (U) $IICB^{Glc}$ activity, (V) PGI activity, (W) G6PD activity, (X) PFKA/FBP activities (Y) PYKF and PPSA activity, (Z) CS activity, (AA) KGDH activity, (AB) PEPC/PCK activity, (AC) ICL activity, (AD) GDH activity. Experimental results are plotted as red lines in (B), (C), (D), and (E). The converted enzyme activities derived from the metabolic fluxes are plotted on the enzyme activity graph using red circles. Green lines show the activity of the reverse reaction, and the net flux values are shown in (X), (Y), and (AB).

increased 100-fold in order to get the model to function. Thus, there might have been additional regulation that could not be explained by Cra.

3.3. GLU-production model

GLU is synthesized by a simple biosynthetic pathway from AKG, which is part of the TCA cycle. A GLU producer can easily be obtained by disruption of the AKG dehydrogenase E1 subunit gene (*sucA*) from the wild-type strain (MG1655 Δ*sucA*). In this model, 2-ketoglutarate dehydrogenase (KGDH) expression was attenuated by setting the translation efficiency coefficient, T_{KGDH}, at 0. GLU was defined as being synthesized by GDH alone; although GLU can also be synthesized by the glutamine synthetase-GLU synthase (GS/GOGAT) pathway, the GDH pathway is dominant at high ammonia concentrations (Ikeda et al., 1996). GLU excretion as well as acetate and formate excretion was defined by a mass action equation. We performed a GLU-production experiment by batch culture and a simulation. The cultivation results and metabolic fluxes are shown in Suppl. Fig. 17 and Suppl. Figs. 18–20, respectively, and the complete simulation results of the glucose culture of MG1655 Δ*sucA* are shown in Suppl. Figs 21–24. Some of the results of the simulation are shown in Fig. 4. Although the CO_2 exhaust and acetate excretion were not in good agreement with the experimental results (Fig. 4(C) and (D), respectively), glucose consumption and GLU production showed excellent agreement with the measured profile (Fig. 2(B) and (E)). GLU production was supported by an increased flux of phosphoenolpyruvate carboxylase (PEPC)/phosphoenolpyruvate carboxykinase (PCK) and isocitrate lyase (ICL; Fig. 4(AB) and (AC), respectively), due to a lack of KGDH activity. The reduced cell growth in the GLU producer compared with that of the wild-type strain also contributed to the large amount of GLU excretion.

3.4. Sensitivity analysis

We performed sensitivity analyses for GLU excretion. In the wild-type strain model, the sensitivities of the expression and enzyme parameters were tested against the intracellular GLU concentration. Among the expression parameters, the translation efficiency of KGDH had the most negative effect on the intracellular GLU concentration. Among the enzyme parameters, the catalytic constant (k_{cat}) of KGDH had the greatest effect on the intracellular GLU concentration. These findings imply that the model can describe the importance of KGDH activity in GLU biosynthesis. In a GLU-producing model in which the KGDH activity was attenuated, the parameter that had the most negative influence on the extracellular GLU concentration among all of the enzyme parameters and expression parameters was the decay constant of *gltA* mRNA, which directly governs the flux to the TCA cycle via citrate synthase (CS) activity. The most negative enzymatic parameter against the extracellular GLU concentration was the k_{cat} of ICL, which catalyzes the glyoxylate shunt reaction at the branch point of isocitrate (ICIT).

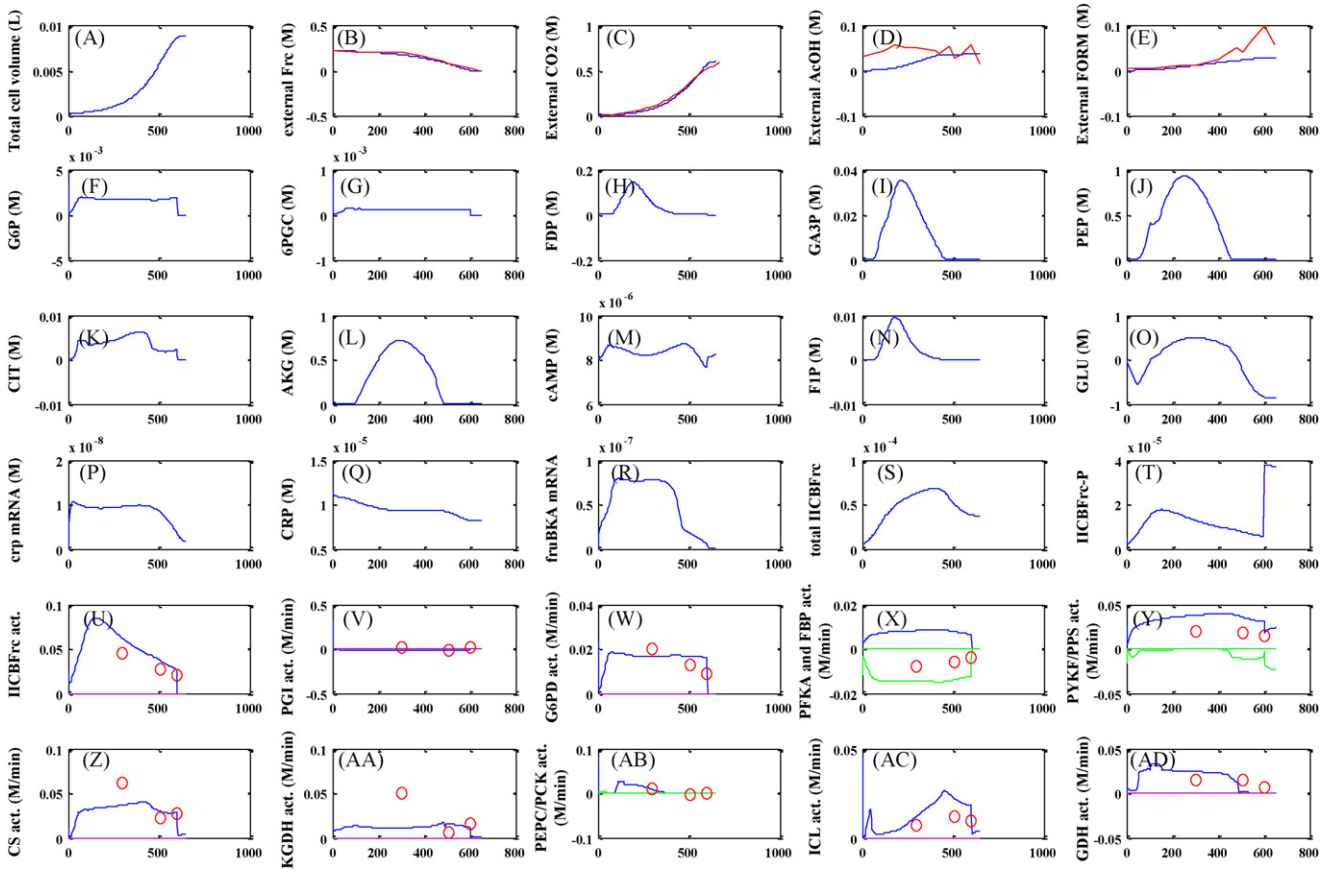

Fig. 3. Simulation of fructose culture of *E. coli* wild-type strain MG1655. (A) Total cell volume, (B) external FRC, (C) external CO_2, (D) external AcOH, (E) external FORM, (F) G6P, (G) 6PGC, (H) FDP, (I) GA3P, (J) PEP (K) CIT, (L) AKG, (M) cAMP, (N) F1P, (O) GLU, (P) *crp* mRNA, (Q) CRP, (R) *fruBAK* mRNA, (S) $IICB^{Frc}$, (T) $IICB^{Frc}$-P, (U) $IICB^{Frc}$ activity, (V) PGI activity, (W) G6PD activity, (X) PFKA/FBP activities (Y) PYKF and PPSA activity, (Z) CS activity, (AA) KGDH activity, (AB) PEPC/PCK activity, (AC) ICL activity, (AD) GDH activity. Experimental results are plotted as red lines in (B), (C), (D), and (E). The converted enzyme activities derived from the metabolic fluxes are plotted on the enzyme activity graph using red circles. Green lines show the activity of the reverse reaction, and the net flux values are shown in (X), (Y), and (AB).

3.5. Simulation of malic enzyme gene activation by malate

In order to show that the constructed simulation system was useful for *in silico* experiments, we tested the hypothesis of repression of the genes *sfcA* for malic enzyme (NAD) (NADME) and b2463 for (NADP) (NADPME), which was suggested by Murai et al. (1972), but has not been proven at the molecular level. We assumed that the putative repressor, MalR, represses *sfcA* and b2463, and when MalR binds to malate, the expressions of *sfcA* and b2463 are activated. The rate constant parameters for expression were estimated from the enzyme activity data (Murai et al., 1972), and the malate binding parameters were based on those for other transcription factors (Table 4). The simulation results for both the parental MG1655 Δ*sucA* and the MalR model are shown in Fig. 5. GLU excretion (Fig. 5(J) versus Fig. 5(A)) and *ppc* expression (Fig. 5(M) versus Fig. 5(D) for mRNA; Fig. 5(N) versus Fig. 5(E) for enzyme), were not affected by MalR regulation; however, expression of the malic enzyme genes (Fig. 5(P) versus Fig. 5(G) for mRNA; Fig. 5(Q) versus Fig. 5(H) for enzyme), OAA (Fig. 5(K) versus Fig. 5(B)), and MAL (Fig. 5(L) versus Fig. 5(C)) was drastically changed. Furthermore the enzyme activity profiles of not only malic enzymes (Fig. 5(R) versus Fig. 5(I)) but also PEPC (Fig. 5(O) versus Fig. 5(F)) were close to the experimental results. The fact that the assumption of MalR regulation better explained the experimental results implies the existence of this kind of regulation *in vivo*.

Table 4
Added initial values and parameters for malate activation.

Gene	Module	Parameter	Value	Unit	Reference
malR	Constant	K^{MalR}_{dMAL}	*8.30E−08*	M	
		$[MalR]^{tot}$	*5.00E−04*	M	
sfcA	TF1	K^{MalR}_{dsfcA}	*1.00E−09*	M	
		k^{base}_{sfcA}	*1.00E+04*	$(M\,min)^{-1}$	Murai et al. (1972)
		k^{MalR}_{sfcA}	3.21E+02	$(M\,min)^{-1}$	Murai et al. (1972)
b2463	TF1	K^{MalR}_{db2463}	*1.00E−09*	M	
		k^{base}_{b2463}	9.91E+03	$(M\,min)^{-1}$	Murai et al. (1972)
		k^{MalR}_{b2463}	9.96E+01	$(M\,min)^{-1}$	Murai et al. (1972)

The estimated values are shown in italics.

4. Discussion

In the present study, we constructed a kinetic model of *E. coli* central metabolism and the expression of related genes. In a previous report, we described the behavior of the PTS with respect to the regulation by CRP and Mlc (Nishio et al., 2008). Here we extended the model to *E. coli* central metabolism, including glycolysis, the pentose-phosphate pathway, the TCA cycle, the glyoxylate shunt, the anaplerotic pathway, and GLU and aspartate (ASP) biosynthesis. Furthermore, the regulatory activities of CRP, Mlc, Cra, PdhR, and IclR, which govern *E. coli* central metabolism, are described in the model. As far as we knew the largest-scale kinetic model of *E. coli* central carbon metabolism with experimental validation has been reported by Chassagnole et al. (2002). The enzymatic reactions have been well established, however, the model lacked the TCA-cycle enzymes. Furthermore our model includes gene expression regulated by major transcription factors. In total, 45 enzymatic reactions

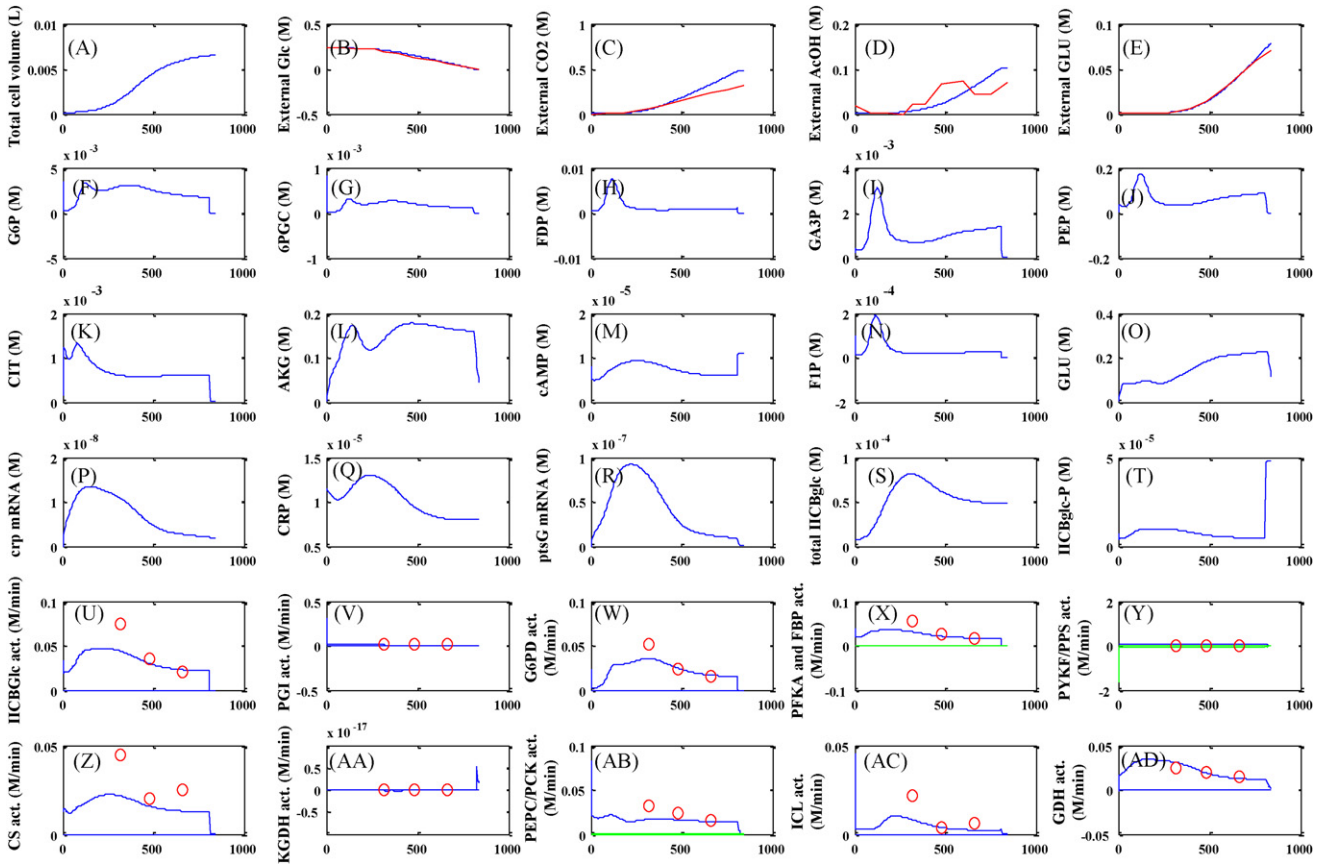

Fig. 4. Simulation of glucose culture of *E. coli* GLU-producing strain MG1655Δ*sucA*. (A) Total cell volume, (B) external GLC, (C) external CO_2, (D) external AcOH, (E) external GLU, (F) G6P, (G) 6PGC, (H) FDP, (I) GA3P, (J) PEP, (K) CIT, (L) AKG, (M) cAMP, (N) F1P, (O) GLU, (P) *crp* mRNA, (Q) CRP, (R) *fruBAK* mRNA, (S) $IICB^{Frc}$, (T) $IICB^{Frc}$-P, (U) $IICB^{Frc}$ activity, (V) PGI activity, (W) G6PD activity, (X) PFKA/FBP activities, (Y) PYKF and PPSA activity, (Z) CS activity, (AA) KGDH activity, (AB) PEPC/PCK activity, (AC) ICL activity, (AD) GDH activity. The experimental results are plotted as red lines in (B), (C), (D), and (E). The converted enzyme activities derived from the metabolic fluxes are plotted on the enzyme activity graph using red circles. Green lines show the activity of the reverse reaction, and the net flux values are shown in (X), (Y), and (AB).

and the expression of 46 genes are incorporated. The expression of the genes is dependent on growth rate defined by the μ values obtained experimentally. Accordingly, our model can describe the transient batch-cultivation production process which is industrially important. We tried to adjust the parameters by taking the experimentally measured external metabolites and metabolic fluxes as representative of *in vivo* enzyme activities. Until now, metabolic fluxes determined by ^{13}C-labeling have been considered the most appropriate values for representing the *in vivo* metabolic state of cells. These are the unique features which are not found in other reports. We believe that our trial using measured metabolic fluxes successfully describes the transient processes occurring during cultivation.

In the wild-type glucose-culture model, we found discrepancies for the enzyme activities of glycolysis and TCA-cycle enzymes (Fig. 2(U), (V), (X), (Z), and (AA)) between the simulation results and the measured activities based on metabolic fluxes at the first sampling time (270 min). These might have been due to the fact that sugar consumption was changing markedly at that time (Fig. 2(B) red line). Thus, the exact sugar-consumption rate might need to be measured. One possible reason for this change was *ptsG* mRNA degradation in response to the intracellular glucose 6-phosphate (G6P) concentration (Kimata et al., 2001; Morita et al., 2003). The decay constant of the *ptsG* mRNA has been reported to change from 0.217 to 2.31 when the intracellular G6P concentration is increased. In our simulation, we investigated this possibility by incorporating a *ptsG* mRNA decay constant change. However, the assumption that intracellular G6P concentrations above 8 mM change the decay constant did not affect the results. A more precise investigation will be needed to clarify whether this system functions to lower the sugar-consumption rate in wild-type cultures.

Wherever possible we attempted to adjust parameters without changing the enzyme kinetic parameters. Thus, we considered the modified enzymatic parameters to be important, because they allowed us to discover the discrepancies between *in vitro* and *in vivo* conditions. Examples were the enzymatic parameters of TALB, TKTI, and MDH, the forward and reverse k_{cat} values, as well as the FBP enzyme parameter, k_{cat}, and the expression parameters, K_{dfbp}^{Cra} and k_{fbp}^{base}, in the fructose culture. Large discrepancies could point to the existence of unknown regulation, or activation or inhibition by metabolites. These observations could lead to new insights into novel *in vivo* regulators.

One example is acetate formation. Under aerobic conditions, excess glucose has been known to cause acetate excretion via phosphotransacetylase (Pta) and acetate kinase (AckA) pathway and acetyl phosphate (acetyl-P) accumulation. As cells begin the transition to stationary phase, cells undergo the metabolic switch and resorb excreted acetate by means of acetyl-CoA synthetase (Acs). Acetyl-P and two components signal transduction pathways have been suggested to be involved to it, however, the mechanism of metabolic switch has not been fully understood (Kumari et al., 2000). Furthermore, all the acetate transport systems have not been identified (Gimenez et al., 2003). Thus we could not construct the acetate uptake model at present time. The metabolic switch was clearly shown in acetate profile of the wild-type glucose culture (Fig. 2D). Similar but unobvious profiles were observed in the fructose culture (Fig. 3D) and the GLU-producing strain culture (Fig. 4D) were probably due to equilibrium between uptake and excretion

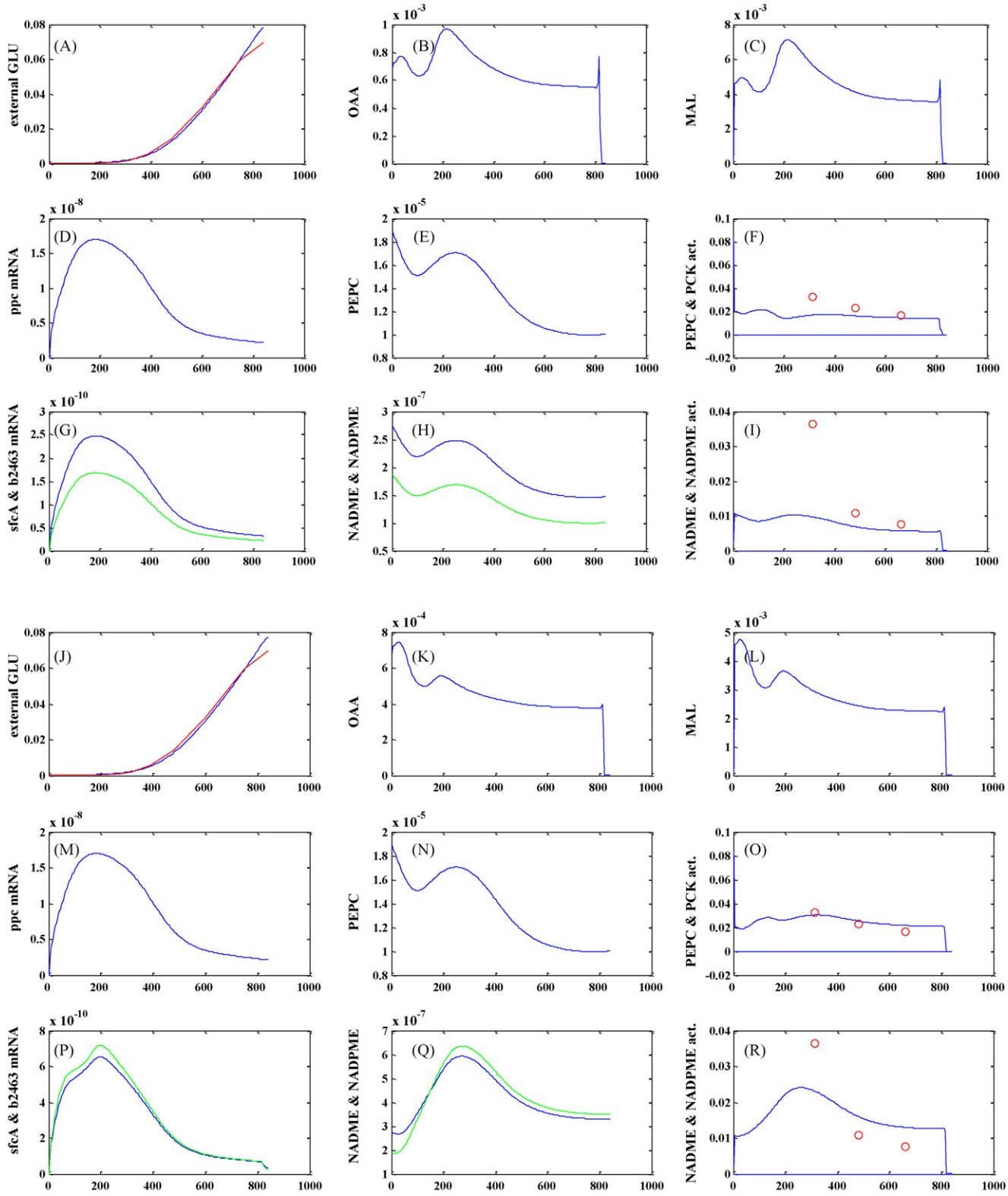

Fig. 5. Simulation of putative regulatory mechanism by the malate repressor. Results for the GLU-producing strain MG1655Δ*sucA*: (A) external GLU, (B) OAA, (C) MAL, (D) *ppc* mRNA, (E) PEPC, (F) PEPC/PCK activity, (G) *sfcA* (blue) and b2463 (green) mRNA, (H) NADME (blue)/NADPME (green), (I) total ME activity. Results for the addition of the putative regulation mechanism to the MG1655Δ*sucA* model, (J) external GLU, (K) OAA, (L) MAL, (M) *ppc* mRNA, (N) PEPC, (O) PEPC/PCK activity, (P) *sfcA* (blue) and b2463 (green) mRNA, (Q) NADME (blue)/NADPME (green), (R) total ME activity. The experimental results are plotted as red lines in (A) and (J). The converted enzyme activities derived from metabolic fluxes are plotted on the enzyme activity graph using red circles in (F), (I), (O), and (R).

in the low acetate concentration. If acetate uptake is appropriately modeled, acetate profile can be simulated more precisely.

Gene expression, enzyme activities, intracellular metabolite concentrations, and metabolic fluxes of the *E. coli sucA* mutant have been analyzed previously (Li et al., 2006). Here we found similar metabolic fluxes resulting in increased PP pathway, glyoxylate shunt, PEPC-PCK, and malic enzyme fluxes (Suppl. Fig. 2 for the wild-type and Suppl. Fig 18 for the Δ*sucA* strain). Li et al. (2006) reported TPI and PGK up-regulation, and PFK, FBA, and PYK down-regulation, from measurements of enzyme activity, and we up-regulated PFK and FBA in our simulation. However, probably due to different cultivation conditions, Li et al. did not detect a large amount of GLU excretion in the Δ*sucA* strain derived from BW25113.

We found that the intracellular GLU concentration was high in the wild-type cell simulation; however, we did not detect excretion of a large amount of GLU into the medium in the wild-type culture. In *C. glutamicum*, *odhA*, which corresponds to *sucA* in *E. coli*, has been cloned (Usuda et al., 1996), and *odhA* disruptants have been reported to produce GLU (Asakura et al., 2007). Recently, additional mutations in the mechanosensitive channel homolog gene (NCgl1221) have been suggested to be necessary for constitutive GLU secretion (Nakamura et al., 2007). These facts imply that an *E. coli* MG1655 Δ*sucA* strain might also carry additional mutations that are involved in GLU excretion. The high intracellular GLU concentration in an MG1655 Δ*sucA* strain might lead to mutation(s) in a gene encoding GLU exporter with high K_m or mutation(s) which provide(s) increased expression of GLU exporter.

In the current study, sensitivity analyses were performed, and the results appeared to be reasonable based on previous findings. To investigate new factors involved in GLU production, extensive and detailed sensitivity analyses are required, and are now underway. *In silico* experiments assuming a malate repressor could suggest the existence of regulation by malate. The hypotheses generated from the gaps between the simulation and experimental results need be tested and validated carefully with further experiments and iterative simulation; this should provide critical information about the present bottlenecks affecting producing strains. Further extension and development of the model to higher accuracy, and the integration of the simulation system with measurements other than metabolic fluxes, is expected to provide a new tool for the rational improvement and design of metabolic and regulatory networks.

Nomenclature

Metabolites

13DPG	1,3-bis-phosphoglycerate
2PG	2-phosphoglycerate
3PG	3-phosphoglycerate
AcCoA	acetyl-CoA
AcOH	acetate
AKG	α-ketoglutarate
ASP	aspartate
cAMP	cyclic AMP
CIT	citrate
D6PGC	D-6-phosphate-gluconate
D6PGL	D-6-phosphate-glucono-delta-lactone
DHAP	dihydroxyacetone phosphate or glycerone phosphate
E4P	erythrose 4-phosphate
F1P	fructose 1-phosphate
F6P	fructose 6-phosphate
FDP	fructose 1,6-diphosphate
FORM	formate
FRC	fructose
FUM	fumarate
G6P	glucose 6-phosphate
GA3P	glyceraldehyde 3-phosphate
GLC_{xt}	external D-glucose
GLU	glutamate
ICIT	isocitrate
MAL	malate
OAA	oxaloacetate
PEP	phosphoenolpyruvate
PYR	pyruvate
Q	ubiquinone
QH_2	ubiquinol
R5P	ribose 5-phosphate
RL5P	D-ribulose 5-phosphate
S7P	sedo-heptulose 7-phosphate
SUCC	succinate
SUCCoA	succinyl-CoA
TCA	tricarboxylic acid
X5P	D-xylulose-5-phosphate

Enzyme and transcriptional factors

6PGD	6-phosphogluconate dehydrogenase
ASPAT	aspartate transaminase
ACNA	aconitase A
ACNB	aconitase B
Cra	catabolite repressor/activator
CDP	cAMP phosphodiesterase
CRP	cyclic AMP receptor protein
CS	citrate synthase
CYA	adenylate cyclase
dGPM	phosphoglycerate mutase 1
ENO	enolase
FBA	fructose-1,6-bisphosphate aldolase class II
FBP	fructose-1,6-bisphosphatase
FRD	fumarate reductase
FRUK	fructose-1-phosphate kinase
FUMA	fumarase A
G6PD	glucose 6-phosphate-1-dehydrogenase
GAPA	glyceraldehyde-3-phosphate dehydrogenase-A
GDH	glutamate dehydrogenase
ICDH	isocitrate dehydrogenase
ICDP/ICDK	isocitrate dehydrogenase kinase/phosphatase
ICL	isocitrate lyase
IclR	acetate operon repressor
iGPM	phosphoglycerate mutase 1
KGDH	2-ketoglutarate dehydrogenase
MDH	malate dehydrogenase
Mlc	making large colonies protein
MQO	malate:quinone oxidoreductase
MSA	malate synthase A
NADME	malic enzyme (NAD)
NADPME	malic enzyme (NADP)
PCK	phosphoenolpyruvate carboxykinase
PDH	pyruvate dehydrogenase
PdhR	pyruvate dehydrogenase complex repressor
PEPC	phosphoenolpyruvate carboxylase
PFKA	phosphofructokinase
PGI	phosphoglucose isomerase
PGK	phosphoglycerate kinase
PGL	6-phosphogluconolactonase
PPS	phosphoenolpyruvate synthase
PTS	phosphotransferase system, consisting of EI, HPr, IIA^{Glc}, and $IICB^{Glc}$
PKI	pyruvate kinase I
RPE	ribulose phosphate 3-epimerase
RPIA	ribose-5-phosphate isomerase A
SCS	succinyl-CoA synthetase

SDH	succinate dehydrogenase
TALB	transaldolase B
TKTI	transketolase I
TKTII	transketolase II
TPI	triosephosphate isomerase

Acknowledgments

We thank Hiroshi Matsui, Yusuke Nakazawa, and Daisuke Shimazaki of Kyoto Prefectural University, Japan, for kinetic data on the enzymes, Yohei Yamada and Takayuki Tanaka for useful discussions, and Professor Tadashi Masuda of Tokyo Medical and Dental University for valuable advices. The authors are also grateful to Mai Shimazaki and Fumiko Yamamoto, and to Hiroyuki Aoyagi for excellent technical assistance.

Appendix A. Supplementary data

Supplementary data associated with this article can be found, in the online version, at doi:10.1016/j.jbiotec.2010.02.018.

References

Asakura, Y., Kimura, E., Usuda, Y., Kawahara, Y., Matsui, K., Osumi, T., Nakamatsu, T., 2007. Altered metabolic flux due to deletion of odhA causes L-glutamate overproduction in *Corynebacterium glutamicum*. Appl. Environ. Microbiol. 73, 1308–1319.

Bongaerts, J., Kramer, M., Muller, U., Raeven, L., Wubbolts, M., 2001. Metabolic engineering for microbial production of aromatic amino acids and derived compounds. Metab. Eng. 3, 289–300.

Bremer, H., Dennis, P.P., 1996. Modulation of chemical composition and other parameters of the cell by growth rate. In: Neidhardt, F.C., et, al. (Eds.), *Escherichia coli* and *Salmonella*: Cellular and Molecular Biology, 2nd ed. American Society for Microbiology, Washington, DC, pp. 1553–1569.

Chassagnole, C., Noisommit-Rizzi, N., Schmid, J.W., Mauch, K., Reuss, M., 2002. Dynamic modeling of the central carbon metabolism of *Escherichia coli*. Biotechnol. Bioeng. 79, 53–73.

de Graaf, A.A., Eggeling, L., Sahm, H., 2001. Metabolic engineering for L-lysine production by *Corynebacterium glutamicum*. Adv. Biochem. Eng. Biotechnol. 73, 9–29.

Gimenez, R., Nuñez, M.F., Badia, J., Aguilar, J., Baldoma, L., 2003. The gene *yjcG*, cotranscribed with the gene *acs*, encodes an acetate permease in *Escherichia coli*. J. Bacteriol. 185, 6448–6455.

Goryanin, I.I., Lebedeva, G.V., Mogilevskaya, E.A., Metelkin, E.A., Demin, O.V., 2006. Cellular kinetic modeling of the microbial metabolism. Methods Biochem. Anal. 49, 437–488.

Ikeda, T.P., Shauger, A.E., Kustu, S., 1996. *Salmonella typhimurium* apparently perceives external nitrogen limitation as internal glutamine limitation. J. Mol. Biol. 259, 589–607.

Imaizumi, A., Kojima, H., Matsui, K., 2006. The effect of intracellular ppGpp levels on glutamate and lysine overproduction in *Escherichia coli*. J. Biotechnol. 125, 328–337.

Ishii, N., Robert, M., Nakayama, Y., Kanai, A., Tomita, M., 2004. Toward large-scale modeling of the microbial cell for computer simulation. J. Biotechnol. 113, 281–294.

Iwatani, S., Van Dien, S., Shimbo, K., Kubota, K., Kageyama, N., Iwahata, D., Miyano, H., Hirayama, K., Usuda, Y., Shimizu, K., Matsui, K., 2007. Determination of metabolic flux changes during fed-batch cultivation from measurements of intracellular amino acids by LC–MS/MS. J. Biotechnol. 128, 93–111.

Iwatani, S., Yamada, Y., Usuda, Y., 2008. Metabolic flux analysis in biotechnology processes. Biotechnol. Lett. 30, 791–799.

Jishage, M., Iwata, A., Ueda, S., Ishihama, A., 1996. Regulation of RNA polymerase sigma subunit synthesis in *Escherichia coli*: intracellular levels of four species of sigma subunit under various growth conditions. J. Bacteriol. 178, 5447–5451.

Karp, P.D., Keseler, I.M., Shearer, A., Latendresse, M., Krummenacker, M., Paley, S.M., Paulsen, I., Collado-Vides, J., Gama-Castro, S., Peralta-Gil, M., Santos-Zavaleta, A., Penaloza-Spinola, M.I., Bonavides-Martinez, C., Ingraham, J., 2007. Multidimensional annotation of the *Escherichia coli* K-12 genome. Nucleic Acids Res. 35, 7577–7590.

Kimata, K., Tanaka, Y., Inada, T., Aiba, H., 2001. Expression of the glucose transporter gene, *ptsG*, is regulated at the mRNA degradation step in response to glycolytic flux in *Escherichia coli*. EMBO J. 20, 3587–3595.

Kimura, E., 2003. Metabolic engineering of glutamate production. Adv. Biochem. Eng. Biotechnol. 79, 37–57.

Kumari, S., Beatty, C.M., Browning, D.F., Busby, S.J.W., Simel, E.J., Hovel-Miner, G., 2000. Regulation of acetyl coenzyme A synthetase in *Escherichia coli*. J. Bacteriol. 182, 4173–4179.

Lee, S.B., Bailey, J.E., 1984. Analysis of growth rate effects on productivity of recombinant *Escherichia coli* populations using molecular mechanism models. Biotech. Bioeng. 26, 66–72.

Leuchtenberger, W., Huthmacher, K., Drauz, K., 2005. Biotechnological production of amino acids and derivatives: current status and prospects. Appl. Microbiol. Biotechnol. 69, 1–8.

Li, M., Ho, P.Y., Yao, S., Shimizu, K., 2006. Effect of *sucA* or *sucC* gene knockout on the metabolism in *Escherichia coli* based on gene expressions, enzyme activities, intracellular metabolite concentrations and metabolic fluxes by ^{13}C-labeling experiments. Biochem. Eng. J. 30, 286–296.

Morita, T., El-Kazzaz, W., Tanaka, Y., Inada, T., Aiba, H., 2003. Accumulation of glucose 6-phosphate or fructose 6-phosphate is responsible for destabilization of glucose transporter mRNA in *Escherichia coli*. J. Biol. Chem. 278, 15608–15614.

Murai, T., Tokushige, M., Nagai, J., Katsuki, H., 1972. Studies on regulatory functions of malic enzymes. I. Metabolic functions of NAD- and NADP-linked malic enzymes in *Escherichia coli*. J. Biochem. (Tokyo) 71, 1015–1028.

Nakamura, J., Hirano, S., Ito, H., Wachi, M., 2007. Mutations of the *Corynebacterium glutamicum* NCgl1221 gene, encoding a mechanosensitive channel homolog, induce L-glutamic acid production. Appl. Environ. Microbiol. 73, 4491–4498.

Neidhardt, F.C., Umbarger, H.E., 1996. Chemical composition of *Escherichia coli*. In: Neidhardt, F.C., et, al. (Eds.), *Escherichia coli* and *Salmonella*: Cellular and Molecular Biology, 2nd ed. American Society for Microbiology, Washington, DC, pp. 13–16.

Nishio, Y., Usuda, Y., Matsui, K., Kurata, H., 2008. Computer-aided rational design of the phosphotransferase system for enhanced glucose uptake in *Escherichia coli*. Mol. Syst. Biol. 4, 160.

Ovádi, J., Srere, P.A., 1996. Metabolic consequences of enzyme interactions. Cell Biochem. Funct. 14, 249–258.

Pramanik, J., Keasling, J.D., 1997. Stoichiometric model of *Escherichia coli* metabolism: incorporation of growth-rate dependent biomass composition and mechanistic energy requirements. Biotechnol. Bioeng. 56, 398–421.

Rohwer, J.M., Meadow, N.D., Roseman, S., Westerhoff, H.V., Postma, P.W., 2000. Understanding glucose transport by the bacterial phosphoenolpyruvate:glycose phosphotransferase system on the basis of kinetic measurements *in vitro*. J. Biol. Chem. 275, 34909–34921.

Sambrook, J., Russell, D.W., 2001. Molecular Cloning A Laboratory Manual, 3rd ed. Cold Spring Harbor Laboratory Press, New York.

Sauer, U., 2006. Metabolic networks in motion: ^{13}C-based flux analysis. Mol. Syst. Biol. 2, 62.

Segel, I.H., 1975. Enzyme Kinetics: Behavior and Analysis of Rapid Equilibrium and Steady-State Enzyme Systems. John Wiley & Sons, New York.

Selinger, D.W., Saxena, R.M., Cheung, K.J., Church, G.M., Rosenow, C., 2003. Global RNA half-life analysis in *Escherichia coli* reveals positional patterns of transcript degradation. Genome Res. 13, 216–223.

Stelling, J., 2004. Mathematical models in microbial systems biology. Curr. Opin. Microbiol. 7, 513–518.

Stephanopoulos, G.N., Aristidou, A.A., Nielsen, J., 1998. Metabolic Engineering: Principles and Methodologies. Academic Press, San Diego.

Usuda, Y., Tujimoto, N., Abe, C., Asakura, Y., Kimura, E., Kawahara, Y., Kurahashi, O., Matsui, H., 1996. Molecular cloning of the *Corynebacterium glutamicum* ('*Brevibacterium lactofermentum*' AJ12036) *odhA* gene encoding a novel type of 2-oxoglutarate dehydrogenase. Microbiology 142, 3347–3354.

Van Dien, S.J., Iwatani, S., Usuda, Y., Matsui, K., 2006. Theoretical analysis of amino acid-producing *Escherichia coli* using a stoichiometric model and multivariate linear regression. J. Biosci. Bioeng. 102, 34–40.

Wang, J., Gilles, E.D., Lengeler, J.W., Jahreis, K., 2001. Modeling of inducer exclusion and catabolite repression based on a PTS-dependent sucrose and non-PTS-dependent glycerol transport systems in *Escherichia coli* K-12 and its experimental verification. J. Biotechnol. 92, 133–158.

Wendisch, V.F., Bott, M., Eikmanns, B.J., 2006. Metabolic engineering of *Escherichia coli* and *Corynebacterium glutamicum* for biotechnological production of organic acids and amino acids. Curr. Opin. Microbiol. 9, 268–274.

Wittmann, C., 2002. Metabolic flux analysis using mass spectrometry. Adv. Biochem. Eng. Biotechnol. 74, 39–64.